NATIONAL AERONAUTICS AND SPACE ADMINISTRATION

Space Programs Summary 37-55, Vol. I

Flight Projects

For the Period November 1 to December 31, 1968

JET PROPULSION LABORATORY
CALIFORNIA INSTITUTE OF TECHNOLOGY
PASADENA, CALIFORNIA

January 31, 1969

NATIONAL AERONAUTICS AND SPACE ADMINISTRATION

Space Programs Summary 37-55, Vol. I

Flight Projects

For the Period November 1 to December 31, 1968

JET PROPULSION LABORATORY
CALIFORNIA INSTITUTE OF TECHNOLOGY
PASADENA, CALIFORNIA

January 31, 1969

SPACE PROGRAMS SUMMARY 37-55, VOL. I

Prepared Under Contract No. NAS 7-100
National Aeronautics and Space Administration

Preface

The Space Programs Summary is a multivolume, bimonthly publication that presents a review of technical information resulting from current engineering and scientific work performed, or managed, by the Jet Propulsion Laboratory for the National Aeronautics and Space Administration. The Space Programs Summary is currently composed of four volumes:

Vol. I. *Flight Projects* (Unclassified)

Vol. II. *The Deep Space Network* (Unclassified)

Vol. III. *Supporting Research and Advanced Development* (Unclassified)

Vol. IV. *Flight Projects and Supporting Research and Advanced Development* (Confidential)

Contents

PLANETARY–INTERPLANETARY PROGRAM

I. *Mariner* Mars 1969 Project

PLANETARY–INTERPLANETARY PROGRAM

A. Introduction

1. Mission Description

The primary objective of the *Mariner* Mars 1969 Project is to make two flyby exploratory investigations of Mars in 1969, which will set the basis for future experiments—particularly those relevant to the search for extraterrestrial life. The secondary objective is to develop Mars mission technology.

The spacecraft design concept is modeled after the successful *Mariner IV* spacecraft, considerably modified to meet the 1969 mission requirements and to enhance mission reliability.

The launch vehicle is the *Atlas/Centaur* SLV-3C, used for the *Surveyor* missions. This vehicle, developed by General Dynamics/Convair Company for the Lewis Research Center, has single- or double-burn capability in its second stage and a considerably increased performance rating over the *Atlas D/Agena D* used in the *Mariner IV* mission.

Mariner Mars 1969 missions will be supported by the Air Force Eastern Test Range, the Deep Space Network, and other NASA facilities.

The six planetary-science experiments selected by NASA for the *Mariner* Mars 1969 missions are listed in Table 1.

2. Project Status

During November and December 1968, systems preparations for the *Mariner* Mars 1969 Project were essentially completed for the final phase of activity prior to launch and the start of flight operations.

The two *Atlas/Centaur* launch vehicles began checkout and testing on the pads of Launch Complex 36. Training and initial test efforts were conducted on the Mission Operations System and the Tracking and Data System, and they were prepared for the final verification and interface tests to be conducted during the immediate prelaunch period.

The spacecraft preshipment review was conducted on December 10 and 11, 1968. The first flight (M69-2) and spare (M69-4) spacecraft were shipped to Cape Kennedy on December 17, 1968. The second flight spacecraft (M69-3) was shipped on January 3, 1969. The proof-test-model spacecraft is being reassembled and will be stationed at the JPL Spacecraft Assembly Facility to provide support during final operational testing and flight operations.

Table 1. *Mariner* Mars 1969 science experiments and investigations

Experiment	Investigator	Affiliation
Television	R. B. Leighton[a]	CIT
	B. C. Murray	CIT
	R. P. Sharp	CIT
	N. H. Horowitz	CIT
	A. G. Herriman	JPL
	R. K. Sloan	JPL
	M. E. Davies	Rand Corp.
	C. Leovy	University of Washington
	B. A. Smith	New Mexico State University
Infrared spectrometer	G. C. Pimentel[a]	UCB
	K. C. Herr	UCB
Ultraviolet airglow spectrometer	C. A. Barth[a]	University of Colorado
	F. C. Wilshusen	University of Colorado
	K. Gause	University of Colorado
	K. K. Kelly	University of Colorado
	R. Ruehle	University of Colorado
	J. B. Pearce	University of Colorado
	E. F. Mackey	Packard-Bell Electronics Corp.
	W. G. Fastie	Johns Hopkins University
Infrared radiometer	G. Neugebauer[a]	CIT
	G. Munch	CIT
	S. C. Chase	Santa Barbara Research Center, Hughes Aircraft Co.
S-band occultation	A. J. Kliore[a]	JPL
	G. Fjeldbo	Stanford University/JPL
	S. I. Rasool	Goddard Institute of Space Studies
Celestial mechanics	J. D. Anderson[a]	JPL
	W. L. Martin	JPL

[a]Principal Investigator.

Revision of mission operations planning documents, such as the Mission Plan and Requirements document and the Coordinated Operations Plan, were underway, and definitive planning of Cape Kennedy and postlaunch operations was carried out. The Tenth Project Quarterly Review was held December 12, 1968.

B. Project Engineering

1. Spacecraft System Test and Prelaunch Operations

a. Introduction. Mariner Mars 1969 spacecraft system test and prelaunch operations progressed on schedule during November and December 1968 (SPS 37-50, Vol. I, Fig. 10, p. 42). During this period, all JPL Pasadena test operations for the flight spacecraft (M69-2 and M69-3) and the flight spare spacecraft (M69-4) were completed.

b. Spacecraft M69-2

Postenvironmental disassembly and cleaning. Following the completion of environmental testing in October, spacecraft M69-2 was disassembled to the lowest level achievable by demating connectors. It was then examined microscopically for physical damage incurred during previous handling and testing and selected units were returned to subsystem laboratories for margin testing and calibration.

Cleaning and reassembly. Spacecraft hardware was cleaned and reassembled during the period November 4–8. All cleaning and assembly operations were performed in specially prepared clean rooms in the Spacecraft Assembly Facility (SAF) high-bay area.

Scan control subsystem telemetry calibration. A scan control subsystem telemetry calibration was performed during the period November 11–13 to provide accurate data concerning the correlation between the telemetered scan platform position data and the actual position of the scan platform cone and clock planes.

Scan platform instrument alignment verification. In conjunction with the scan telemetry calibration, a scan platform instrument alignment verification was performed. The line-of-sight of each planetary instrument was measured with respect to a reference plane on the scan platform.

System test 3. Spacecraft M69-2 system test 3 was conducted on November 15–26. The purpose of the test was to verify the functional performance of the spacecraft as an integrated system within the constraints imposed by test equipment and the earth-based environment. During the test, the spacecraft was operated in all major modes of the nominal flight sequence.

Shipment to the Air Force Eastern Test Range. Preparation for shipment of the spacecraft to the Air Force Eastern Test Range (AFETR) began after completion of system test 3 in late November and continued through the first half of December. Preparation included the removal of certain delicate hardware (e.g., gyroscopes) for separate shipment by aircraft.

The spacecraft left JPL on December 17 in an escorted convoy of four air-ride electronics moving vans and arrived at the AFETR on December 21. Following arrival

at the AFETR Spacecraft Checkout Facility (SCF), Building AO, a careful visual inspection of the spacecraft was performed. The spacecraft was then installed on its low-level positioner in the SCF high-bay and stored until the start of mechanical operations in January 1969.

c. Spacecraft M69-3

Vibration test. Spacecraft M69-3 vibration testing was conducted during the period October 31–November 1 in the JPL Environmental and Dynamics Test Laboratory. The purpose of the test was to verify that the spacecraft could operate satisfactorily during and after exposure to the vibration levels based upon those of the *Atlas/Centaur* launch vehicle.

Pyrotechnic shock test. The pyrotechnic shock test was performed immediately after completion of the vibration test, while the spacecraft was still installed on the spacecraft adapter. The spacecraft adapter V-band pyrotechnics were detonated and the resulting shocks were measured with instrumentation accelerometers.

Scan platform instrument alignment verification. Scan platform instrument alignments were verified on spacecraft M69-3 during the period November 5–6. The line-of-sight of each planetary instrument was measured.

System test 2. During the period November 7–13, spacecraft M69-3 system test 2 was conducted to verify the functional performance of the spacecraft as an integrated system. All major parts of the nominal flight sequence were tested, including several types of encounter sequences and trajectory-correction maneuvers.

Postenvironmental disassembly and inspection. The spacecraft was disassembled and inspected for physical damage during the period November 13–20. Selected units were returned to subsystem laboratories for special testing and calibration.

Cleaning and reassembly. Spacecraft components were cleaned and reassembled in specially prepared clean rooms in the SAF high-bay area during the period November 21–27.

Scan control subsystem telemetry calibration. Calibration of the scan control subsystem telemetry channels was performed during the period December 2–4 to accurately determine the correlation between the telemetered scan platform position data and the actual position of the scan platform.

System test 3. Spacecraft M69-3 system test 3 was performed on December 5–20 to verify functional integrity of the spacecraft as a system following postenvironmental disassembly and inspection. The test included all system test exercises not previously performed.

Preparation for shipment to the AFETR. Preparation for shipment of the spacecraft to the AFETR continued through the remainder of December. Certain delicate equipment were removed from the spacecraft for separate shipment.

d. Spacecraft M69-4

Space simulation test, part I. Part I of the space simulation test was performed in the JPL 10-ft space simulator during the period October 31–November 10. The purpose of part I was to demonstrate long-term (about 250 h) spacecraft functional performance while operating in a simulated space environment. Each of the key segments of the flight sequence was repeated several times during the test. The nominal environment for the test was a pressure of less than 5×10^{-5} torr and a space simulator cold-wall temperature of about $-300°F$.

Space simulation test, part II. Preparation for space simulation test, part II, was performed during the period November 10–13. Preparation included removal of externally mounted test equipment, test cables, and other hardware that could interfere with the compilation of accurate temperature control data.

The objective of space simulation test, part II (November 13–22), was to verify the spacecraft temperature control subsystem design. In addition, real-time 33-, 33-, and 17-picture encounter sequences were performed.

Partial disassembly and reassembly. A partial disassembly of the spacecraft for margin testing of key equipment was performed during the period November 22–23. After completion of the margin tests, the equipment and the spacecraft were reassembled to the system test configuration during the period November 23–26.

System test 2. System test 2, the final system test at JPL, was performed on November 26–December 6. The purpose of the test was to verify the functional performance of the spacecraft as an integrated system. All significant portions of the nominal flight sequence were tested.

Shipment to AFETR. Spacecraft M69-4 was readied for shipment to the AFETR on December 9–16. The spacecraft left JPL on December 17 in an escorted convoy of four air-ride electronics moving vans. (Spacecraft M69-2 was shipped in the same convoy.) The convoy arrived at the AFETR on December 21.

Arrival Inspection and Assembly. After arrival at the AFETR Explosive Safe Facility, a careful visual inspection of the spacecraft was performed. The spacecraft was then installed on its low-level positioner inside a portable laminar downflow clean room. Assembly operations were performed during the remainder of December in preparation for the start of electrical testing in early January 1969.

C. Systems

1. Mission Operations

Training and testing activities for *Mariner* Mars 1969 mission operations personnel has continued on an accelerated schedule through the months of November and December 1968. Command exercises were conducted with Echo DSS on November 15, Woomera DSS on November 26, Johannesburg DSS on December 4, and Cebreros DSS on December 16. The primary purpose of these tests was to demonstrate the capabilities of the spacecraft performance analysis and command group, mission control, and DSN personnel (and their hardware and software) to generate, verify, and transmit commands to a simulated spacecraft in accordance with established command procedures.

On November 14, 1968, the Maneuver-Spacecraft-G/Cruise-Spacecraft-F Test, the last mission operations training plan test, was conducted. This was the first test in which simulated data from two spacecraft was processed and displayed by the real-time telemetry system in the Space Flight Operations Facility. No significant problems in either the software or hardware systems were encountered, and minor procedural problems that occurred have since been corrected.

The last major test performed during this period was a system training test – Launch G. This test, performed on December 19, 1968, was the first system-level test involving active participation by the DSSs. (The Johannesburg DSS, Cebreros DSS, and Cape Kennedy compatibility test station were involved in the simulated launch activities.) Test objectives were to familiarize *Mariner* Mars 1969 operations personnel with the sequence of events expected to be used during actual space flight operations, and to determine the adequacy of the resources committed to *Mariner* Mars 1969 to support the launch phase of the mission. No significant difficulties were encountered although the sequence of events list will continue to be updated and modified as new information is obtained.

During the Maneuver-Spacecraft-G/Cruise-Spacecraft-F exercise on November 14, and in the Launch G exercise on December 19, the source of the simulated telemetry data was the Phase IA simulation program developed for the EMR 6050 computer. As a result of the tests, a definite improvement in simulated data has been established over recorded analog tape simulation used on some former projects.

In addition to the mission operations training and test activities described above, a series of design compatibility tests were conducted during the period November 14–22. These tests were conducted between the M69-4 flight spacecraft, while located in the space simulator, and various elements of mission operations.

The first test was to demonstrate that the real-time telemetry data system could accept, process, and display, in the spacecraft performance analysis area, selected flight spacecraft telemetry data.

The next test, a spacecraft-coded command data test, was to demonstrate that coded commands, produced by the COMGEN program, could be transmitted to a flight spacecraft by the command data system along with selected quantitative and direct commands.

The third, and last, test of this series was an operational compatibility test, the objectives of which were to demonstrate that the ground system, including personnel, could operate a flight spacecraft in accordance with selected portions of the sequence of events list and to demonstrate that the sequence could be executed. This was a three-day test in which an encounter sequence planned for the Cruise-Spacecraft-F test was executed in real time through the far- and near-encounter sequences. In addition, all expected playback modes were exercised. The only design compatibility problems experienced during these tests were procedural in nature.

2. UNIVAC 1219 Data Processing System

Programming and hardware development efforts were conducted during this period to enable the use of both the UNIVAC 1219/1218 computer systems and the TV

ground data handling system (TV-1) for processing and displaying the *Mariner* Mars 1969 TV subsystem calibration data. The encoded data from TV subsystem calibration is derived simultaneously from the following four sources:

(1) Digitized full analog video (FAV).

(2) Digitized composite analog video (CAV), which embodies the cubing and AGC functions performed on the FAV.

(3) Digital video (DV), which consists of every-seventh-element data digitized by the TV subsystem.

(4) The 1/28th sampled pixel data.

All the data bits and the associated bit sync, line sync, and frame sync pulses are recorded on a 14-track Ampex CP-100 magnetic tape recorder during TV calibration. The data processing function, consisting mainly of data translation, assembles the FM-recorded samples from these various sources to provide line- and frame-synchronized data on digital magnetic tape in a form suitable for processing on a digital computer. This function is accomplished in the first step of a three-pass processor, in which the data bits and sync pulses are conditioned by special tape-reproducer interface hardware. The hardware provides numerous adjustments for compensating skew of the data bits, setting noise threshold, etc. The UNIVAC 1219 computer identifies and time-tags the data and produces a digital log tape output.

The log tape is subsequently processed to provide a master record with data discrepancies identified, such as missing data or sync pulses, time anomalies, etc. The master record can then be used to drive TV-1 to produce quick-look pictures of the calibration data, and also to provide four separate types of formatted tapes for processing by the image processing laboratory (IPL). Each tape contains only FAV, CAV, DV, or 1/28th element data. In the future, it may be expedient to use the master record tapes as the UNIVAC 1219/IPL interface, rather than the four separate records. The data identification on the master tape is sufficient to enable pixel-by-pixel comparisons of input and output data, or determination of the transfer function between FAV and CAV, etc. These functions were formerly difficult to perform using the four separate tapes formatted by the data analysis facility (DAF) for IPL use.

Difficulty is being experienced with consistent reproduction of the analog tape data, and maintenance is being performed on both Ampex FR-1200 and FR-1800 tape reproducers to attempt to reduce the excessive skew associated with this equipment in this application. The skew problems result in excessive bit errors in the recovered data. Sufficiently consistent results cannot presently be obtained from the reproduce system to permit reliable assessment of the operation of the recording system and the associated TV development support equipment (DSE). Consequently, a large backlog of TV subsystem calibration data has built up, the ultimate processability of which remains somewhat questionable. This backlog was built up during the time that the small computer (PDP-4, Digital Equipment Corp.) in the DAF was being used to process calibration data. The DAF system operation was slow because the analog tape reproduction was run at 1/8 of record speed, and numerous software difficulties were encountered. Design of the software was based on receiving good data, rather than data with the types of deficiencies actually encountered, and computer limitations prevented accomplishing the type of processing of which the UNIVAC 1219 is capable.

The programming of the UNIVAC 1219 system to support testing of the proof test model spacecraft in the Spacecraft Assembly Facility is being completed, and full test support capability is anticipated by January 21, 1969. This capability will consist of the processing and display of: (1) engineering telemetry, (2) CC&S memory (telemetry) dump, (3) spacecraft commands, (4) science real-time telemetry, (5) 86.4 kbits/s high-rate science telemetry (both 972 and 6804-bit formats), (6) 16.2 kbits/s hardline science data (972 bit format), and (7) science playback telemetry (both formats). In addition, capability will be provided for recording the science OSE 18.9 kbyte/s video hardline, and, as previously discussed, all currently available nonreal-time support programs will be used.

D. Engineering Mechanics

1. Temperature Control of the Spacecraft

a. Introduction. The spacecraft temperature control subsystem is required to maintain each component within an acceptable temperature range throughout the duration of the mission. For *Mariner* Mars 1969, this was accomplished by developing a thermal control design based on analysis and previous *Mariner* experience, and then modifying and verifying the design primarily by means of developmental tests on a full-scale thermal control model of the spacecraft. Final verification of the resulting design was accomplished during environmental testing of actual flight spacecraft.

Figure 1 is a photograph of the *Mariner* Mars 1969 spacecraft. From the temperature control point of view, it is convenient to think of this spacecraft as being separable into three main components: spacecraft bus, appendages, and science planetary platform.

The spacecraft bus is an octagon consisting of seven electronic equipment bays and one propulsion bay housing the midcourse correction motor and its tankage. The bus also contains the attitude-control (AC) gas tanks, battery, and central tube structure (clock tube) to support and rotate the planetary platform. Appendages are items such as solar panels, antennas, sun sensors, AC gas jets, and other components exterior to the bus–platform envelope.

The science planetary platform contains all of the onboard science instruments and is maneuverable with respect to the spacecraft bus so as to continually orient the instruments toward Mars during encounter. The five instruments mounted to the platform are:

(1) Infrared radiometer (IRR).

(2) Wide-angle TV camera (TV-A).

(3) Ultraviolet spectrometer (UVS).

(4) Narrow-angle TV camera (TV-B).

(5) Infrared spectrometer (IRS).

Also mounted to the platform are a planet sensor, two Mars gates, and the cone actuator motor.

The following discussion of the temperature control subsystem is divided into two sections: (1) The spacecraft bus and appendages. (2) The science planetary platform.

b. Spacecraft Bus and Appendages

Design philosophy. The principal thermal inputs to the spacecraft bus are (1) solar energy absorbed directly or

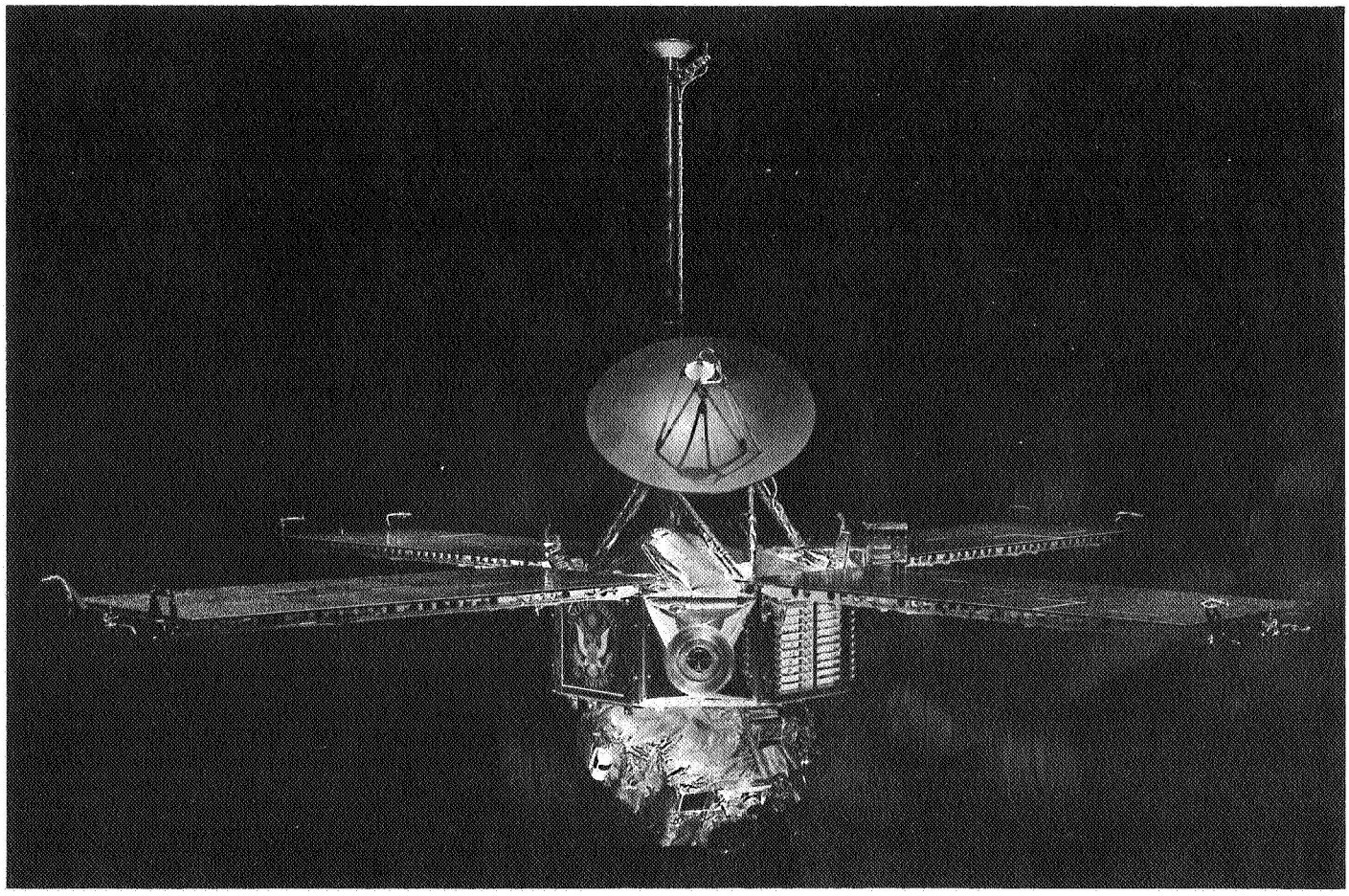

Fig. 1. *Mariner* Mars 1969 spacecraft

re-radiated from the solar panels and absorbed, and (2) internal power dissipation from the electronics. The solar energy flux incident on this sun-oriented spacecraft varies gradually during the course of the mission in a predictable fashion dependent upon the trajectory. The internal power dissipation, on the other hand, can change both level and distribution quite suddenly as various electronic components are switched from one power state to another.

The *Mariner* Mars 1969 temperature control design philosophy varies only slightly from that of previous *Mariner* projects with regard to the bus and appendages. As in the past, this philosophy includes the following tenets:

(1) Isolate the spacecraft as completely as possible from the varying solar input.

(2) Arrange the electronic modules so as to distribute the internal power sources as uniformly as possible throughout the bus.

(3) Minimize thermal gradients within the bus by mounting the electronic subassemblies directly to exterior radiating surfaces and by using high emittance interior surfaces for maximum internal radiant interchange.

(4) Force the heat rejection from the bus to occur only from designated radiator surfaces for which the emittance can be actively controlled by means of temperature control louvers, thereby attenuating the temperature excursions of the bus due to internal power changes.

(5) Rely on the thermal capacitance of the spacecraft to maintain acceptable temperatures during transient periods such as launch and midcourse maneuvers.

(6) Isolate the bus from the platform to eliminate uncertainties in the amount of thermal interchange between them.

Quite often, the distribution of internal power within the spacecraft must be determined by considerations other than those which might optimize thermal design. Table 2 indicates that the distribution within the bus is such that complete bays are without power during some portions of the mission (i.e., bays V and VII except during encounter and/or playback). For this reason, the previous *Mariner* design philosophy has been logically extended to include the use of fixed-resistance ac heaters to provide the bus with substitute power during cruise, thus resulting in a more even distribution of power over the entire mission.

Table 2. Bus internal power distribution[a]

Power mode	Bay I Power/ pyro	Bay II Propulsion	Bay III AC and CC&S	Bay IV Telemetry/ comm	Bay V data storage	Bay VI Radio	Bay VII Science	Bay VIII			Bus total
								Power regulator	Canopus tracker	Clock motor	
Launch to acquisition	25.4	0	50.9	15.6	20.2	84.8	12.5[b]	51.1	0	0	260.5
Midcourse correction maneuver	26.9	0	61.3	15.6	10.0[b]	84.8	12.5[b]	49.4	5.0	0	265.5
Cruise	23.3	0	23.6	15.6	10.0[b]	84.8	12.5[b]	26.4	5.0	0	201.2
Encounter (high TWT power)	21.1	0	23.6	15.6	20.2	111.0	36.7	31.8	5.0	4.7	269.7
Encounter (low TWT power)	21.1	0	23.6	15.6	20.2	84.8	36.7	31.8	5.0	4.7	243.5
Playback (high TWT power)	23.0	0	23.6	15.6	20.2	111.0	12.5[b]	27.4	5.0	0	238.3
Playback (low TWT power)	23.0	0	23.6	15.6	20.2	84.8	12.5[b]	27.4	5.0	0	212.1

[a]Nominal proof test model values (in watts) from thermal data sheets.

[b]Substitute fixed-resistance ac heater power.

The *Mariner* Mars 1969 design philosophy with regard to appendage temperature control is similar to that of previous *Mariner* projects, namely, temperatures are passively controlled, wherever possible, by means of thermal shields and/or appropriate thermo-optical coatings.

Design implementation. Multilayer thermal blankets are employed on both the sunlit (top) and platform (bottom) sides of the spacecraft bus. Both blankets, although of slightly different construction, are designed to provide lightweight, adiabatic boundaries for the bus. The purpose of the top blanket is to isolate the bus from the sun; the bottom blanket's purpose is to minimize thermal gradients within the bus from top to bottom, and to force the internally dissipated power to be rejected to space through the louvered bay faces.

The top blanket is fabricated of 11 layers of mylar film aluminized on both sides by vacuum deposition. These mylar layers are alternated with spacer layers of nylon net, and then sandwiched between two cover layers of 1 mil teflon. The teflon is aluminized on one side and arranged so that the aluminized side faces the blanket interior. The bottom blanket is of similar construction, but utilizes only seven layers of mylar. By facing the teflon side out, the temperature of the sunlit blanket's outer layer is suppressed, and the fragile aluminum surface of the teflon is not subjected to the repeated handling necessary during spacecraft assembly.

The bus power distribution shown in Table 2 indicates that power is dissipated somewhat evenly throughout the bus with the exception of Bay II, which dissipates no power, and Bay VI, which can be a very great power dissipator. All of the electronics in the bus apparently function best at room temperature (70°F), with the exception of the gyros, which require a temperature of 115°F when operating.

For the most part, the factors listed above dictated the thermal configuration of the bay faces. Temperature-control louvers are installed on all of the bays with the exceptions of Bays II, III, and VI. Bay II, because of its lack of power, is covered (with the exception of the nozzle of the midcourse correction motor) with a polished, low-emittance aluminum shield. Bay VI, housing the radio, is painted with high-emittance white paint (PV-100) to reject the large amounts of heat necessary to maintain radio temperatures at a moderate level. Bay III, which houses the gyros, was also covered with a polished aluminum shield to ensure that the gyros reach the elevated temperature they require when operating.

The temperature-control louvers mounted on the remaining bays consist of 22 blades set in 11 horizontal rows, each pair of blades being actuated by a thermally-sensitive bimetallic spring mounted between them. The louver assembly is fabricated from aluminum, the entire external surface being polished to provide a low-emittance shield when the louver blades are closed. The shear plate, or bay face, to which the louver assembly is mounted is painted with high-emittance white paint. As the temperature of the bimetal actuators increases above 60°F, the blades open and allow the rejection of increasing amounts of heat. The louver assembly permits maximum heat rejection when the blades are opened a full 90 deg at a temperature of approximately 85°F.

Since the louver assembly doesn't cover the entire bay face, an area of approximately 120 in.^{2} of white paint remains exposed. During the thermal-vacuum testing of the spacecraft, the bay temperatures can be adjusted somewhat by covering portions of this exposed high-emittance surface with low-emittance, polished aluminum, bolt-on shields. This adjustment ensures that steady-state bay temperatures remain within the louver range throughout the mission.

The interior of the bus is coated with an anodic coating having an emittance of 0.7. Only the centrally located clock tube is polished to help minimize any heat transfer between the bus and scan platform.

Physical distortion is the primary concern with regard to the low- and high-gain antennas. For this reason, the maximum allowable thermal gradient for these items is quite limited, and yet the allowable temperature range is quite large.

The coating used on the sunlit side of the high-gain antenna must be a stable, diffuse reflector to prevent concentration of solar energy on the feed. A green paint (Laminar X-500) was chosen for the sunlit side and "as received" aluminum for the shaded side. The high-gain superstructure is both polished and wrapped with multilayer, tie-on thermal blankets to minimize heat leaks both into and out of the bus.

The low-gain antenna was polished except for the ground plane, which was painted white on the shaded side to minimize the top-to-bottom gradient.

Test results. Each flight spacecraft underwent approximately 500 h of thermal-vacuum testing to verify both the system and temperature control designs. The results

of these tests indicated that, for all practical purposes, the two flight spacecraft and the flight spare are thermally identical. Table 3 summarizes the results of these tests for the first flight spacecraft (M69-3).

The 10-ft diam vacuum chamber in which these tests were conducted was not large enough to include flight-sized solar panels. Shorter dummy solar panels made up of a horizontal heater plate with a small vertical heater plate attached were utilized in place of the real panels. The dummy panels were sized to approximate the proper view factor from the panel to its respective bay. As a result of this space limitation, none of the solar panel tip-mounted hardware were tested during the flight spacecraft tests.

Figure 2 is a plot of total power input to the bus versus average bus temperature for the flight spacecraft. The characteristic operating point for each of the tested mission modes falls along that portion of the plot within the louver actuation range (60–85°F).

For the bus, an appropriate numerical indication of design margin on the low end is the amount of power which must be subtracted from the lowest total power mission mode before the characteristic operating point falls on to the closed-louvers portion of the curve. The lowest power mission mode shown is Mars cruise, indicating a design margin of approximately 56 W on the low end. The corresponding number on the upper end is 135 W.

Table 3. Bus temperature test results in °F

Location	Earth cruise	Mars cruise	TWT low power Mars encounter	TWT high power Mars encounter	TWT high power playback
Bay I	71	66	68	69	67
Bay II	75	64	67	69	67
Bay III	84	73	75	77	76
Bay IV	69	64	66	67	66
Bay V	67	62	65	68	66
Bay VI	68	61	66	82	79
Bay VII	66	62	69	72	66
Bay VIII	69	65	69	69	66
Battery	69	63	67	69	65
AC gas bottles	70	61	68	75	70
Canopus tracker	80	69	72	74	71

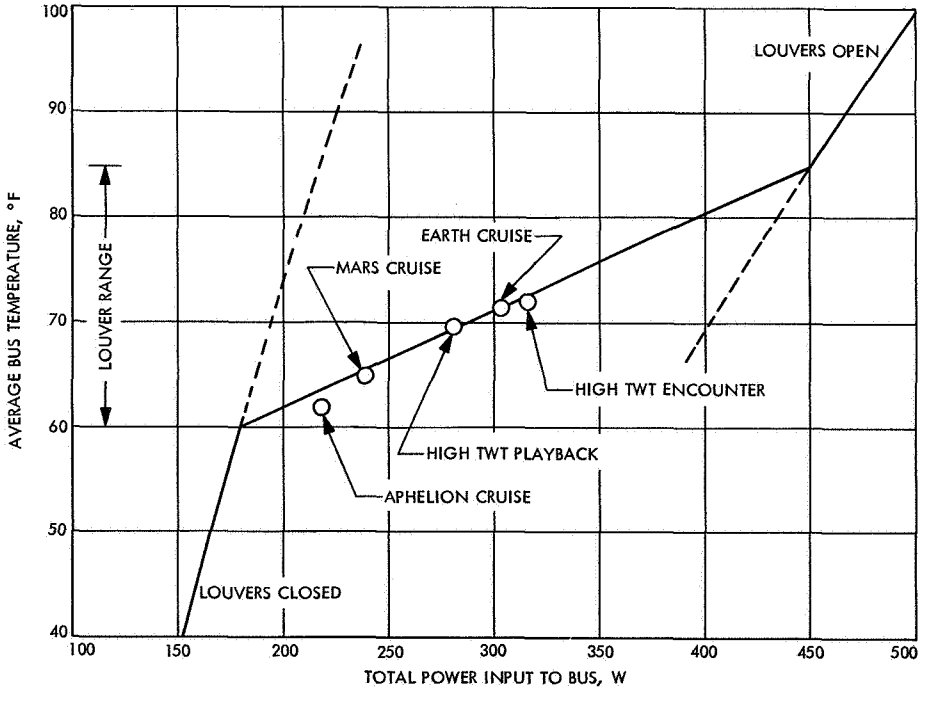

Fig. 2. Bus power versus temperature

Although it appears that the range of average bus temperatures is biased significantly toward the lower end of the louver actuation range, this is not really the case. The total power input to the bus consists of all the various direct solar leaks (i.e., sun sensors, superstructure, blanket seams), internally dissipated power, and long wave-length energy radiated from the backs of the solar panels to the bay faces. This power input from the solar panels is a function not only of the panel temperatures, but also of the particular bay temperature, because it is that bay temperature that determines the angle to which the louver blades open, and, consequently, the amount of energy they will admit to the bay face from the solar panel. Therefore, during an earth cruise when the panels are warm, a given increase in internal power would increase the total power input to the bus by that same amount plus the added input from the solar panels due to the greater louver open angle. Test data indicates that this effect is significant. With all louvers fully open, the solar panels at near-earth temperature (140°F) can input as much as 150 W to the bus.

Test results for certain appendages of the M69-3 (typical) spacecraft are given in Table 4. The sun sensors are adequately slaved to the bus as evidenced by their relatively small cruise temperature excursion and the fact that they drop only to 20°F when the simulated sun is turned off completely. The input to the bus from the sun sensors through the pedestals is minimal – approximately 1.4 W at earth and 1.0 W at Mars. Inputs to, or leaks from, the bus attributable to the other appendage are also minimal. The solar input to the bus, excluding sun sensor inputs, is approximately 30 W at earth and 0 W at Mars.

Table 4. Appendage temperatures as a result of solar input[a]

Appendages	Earth cruise	Mars cruise
Low-gain antenna[b]		
Ground plane	109	23
Center	60	−5
Bus	85	47
High-gain antenna dish[b]		
Maximum	200	80
Minimum	60	−10
Solar panels[b] (average)	140	40
Sun sensors	96	58
AC gas jets[b]	79	1

[a]The temperature values listed are in degrees Fahrenheit.

[b]Data is from either development or thermal control model tests.

Since the primary sun sensors must function in the sun, and must be painted black to minimize optical reflections, the most satisfactory method of maintaining their temperatures within an acceptable range (30–150°F) is to slave them to the bus. The small, solar-dependent heat leak to the bus allowed by this method is of little consequence.

The solar panels are controlled passively by means of a high-emittance, white-painted (Cat-a-Lac) surface on the shadow side to balance the necessary high solar absorptance cell side of the panel. The low solar absorptance of the white paint on the backs of the panels is desired for the transient period during launch when the panels are undeployed and the orientation of the spacecraft is such that the sun strikes the normally-shadowed backs of the panels.

The fact that the solar panels are almost completely sun dependent causes their temperature to decrease approximately 100°F between earth and Mars. Since the acceptable flight temperature of the AC gas jets, solar-panel boost dampers, and pinpullers are similar to those of the solar panels, these items are simply slaved to the panel, properly painted and/or polished to establish their temperature for a given solar intensity, and allowed to be fully solar dependent.

c. Science planetary platform

Design philosophy. Figure 3 shows the location and orientation of the five science instruments, planet sensor, Mars gates, and cone actuator motor on the platform structure. The temperature requirements and power dissipations for the instruments, planet sensor, gates, and actuator are presented in Table 5.

Because the platform is located on the shade side of the spacecraft, the primary thermal input to items located on the platform comes from electrically-dissipated heat within the respective electronics which are operational only during the encounter phase of the mission. When this consideration and the information listed in Table 5 are combined with previous *Mariner* experience, the resulting platform temperature control design philosophy is as follows:

(1) Since radiation and conduction coupling across a complex interface like the platform clock tube is

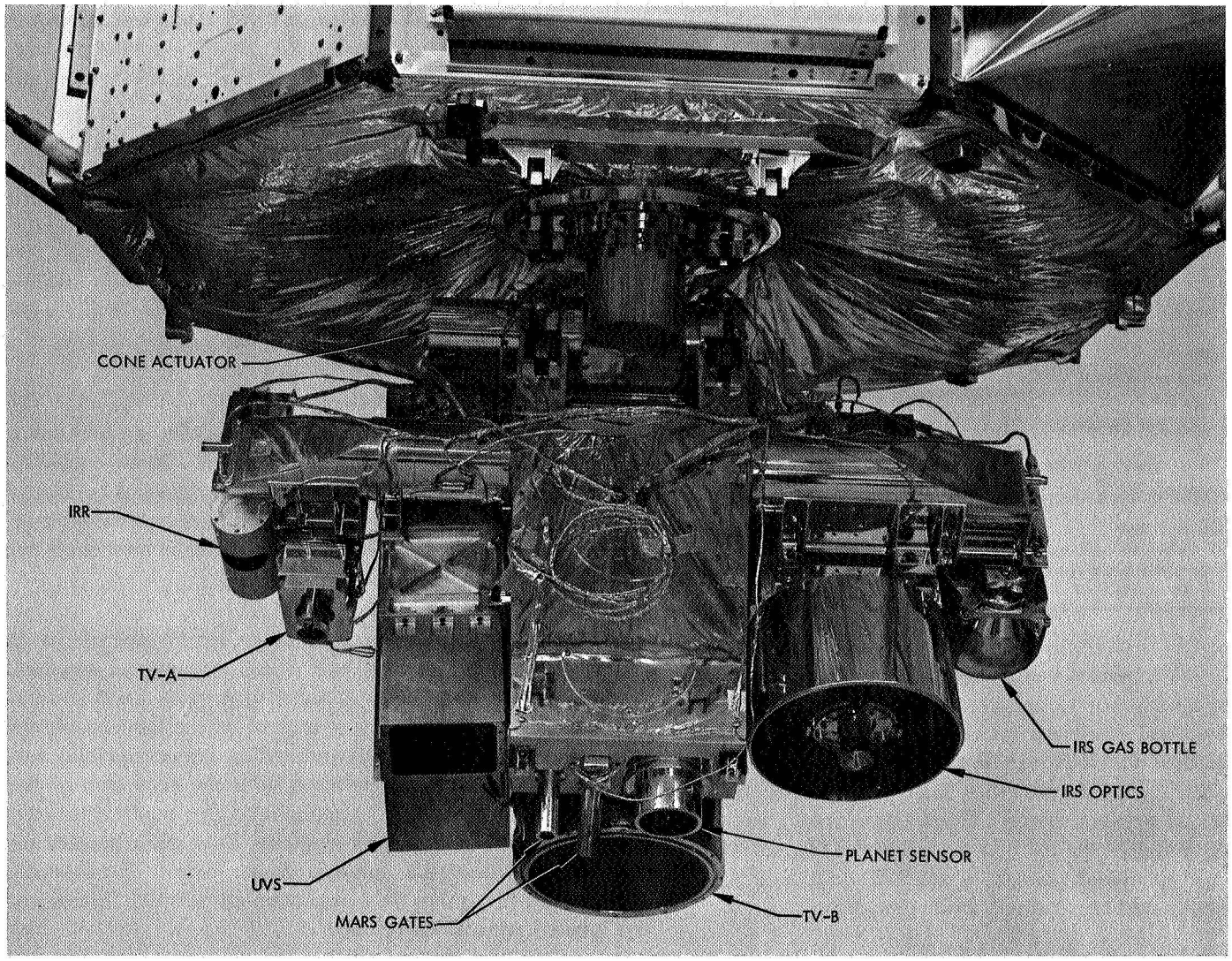

Fig. 3. Equipment location and orientation

unpredictable and non-reproducible, isolate the platform from the bus.

(2) Cluster together those platform items having somewhat common temperature requirements in order to share their dissipated heat, and then insulate the cluster to conserve the heat.

(3) Install heaters[1] in each item to provide approximately the same heat input when non-operative as when operative to maintain relatively uniform power dissipation rates.

(4) Employ permanent heaters to make up deficiencies in power dissipation.

(5) Provide enough design margin to allow for instrument or heater failure.

Design implementation. To achieve thermal decoupling of the platform from the bus, a fiberglass insulating sleeve is used in the clock tube to provide a poor conductive path through the tube. Additionally, the bus end of the tube, as well as most of the platform structure (which is primarily aluminum), is polished to reduce radiation coupling. Test data has demonstrated that good isolation was achieved.

Table 5 shows that a number of items have compatible temperature requirements. If the temperature requirements for TV-A and -B are satisfied, the requirements for

[1]These heaters are called replacement heaters since they replace the power lost when an assembly is turned off.

Table 5. Equipment temperature requirements and power dissipations

Equipment	Required temperature range, °F	Power dissipation, W
IRR	−4–32	2.5
TV-A	−4–86	3.5
UVS	−40–130	14.5
TV-B[a]	−4–86	3.5
IRS		
Monochromator	−54–−27	2.5–7.6
Radiator	−189–−171	0
Cryostat gas bottles	−72–20	0
Planet sensor and Mars gates	−30–125	1.0
Cone actuator	0–167	5.0

[a]The optics barrel gradient should not exceed 4°F during the encounter portion of the mission.

the UVS, planet sensor, Mars gates, and cone actuator are compatible. Consequently, the above items were clustered and insulated within a multilayered blanket. In addition, the IRR was also included within the blanket since its temperature range falls within the above. However, to prevent the IRR temperature from exceeding its upper limit, a cut-out is provided in the blanket to expose a white-painted portion of the IRR to space, and thus provide additional direct heat dissipation.

Replacement heaters are located within each instrument and the cone actuator to maintain the temperature levels and temperature distribution for those items within the blanket in both non-operative and operative modes. The replacement heaters are off when the instruments are operating, and are sized to dissipate approximately the same power as their respective electronics. They are located as close to the source of electronic dissipation as possible.

Though an insulation blanket is employed, not enough energy is conserved to raise the blanketed items to the required temperature levels. Consequently, additional heaters are provided and are permanently on. The permanent heaters within the blanket are the platform heater 1 and the TV-B optics heater. The use of Promethium 147 (a radioisotope) was considered earlier as a substitute for the permanent heaters, but was discarded when it was found that it degraded the performance of the UVS.

In addition to the permanent and replacement heaters for the items within the blanket, a back-up heater is provided. This heater can be ground commanded on and off by a DC-34 command.

Since the effectiveness of an insulating blanket varies from blanket to blanket, and because power variations occur either due to voltage variations or possible equipment failure, an array of louvers is mounted on the UVS through a cut-out in the insulating blanket. These louvers provide additional temperature stabilization of the variable emittance characteristics of the blanketed items.

To illustrate the effect of clustering, consider the example of a replacement heater failure, or perhaps a partial failure of one of the blanketed instruments. The instruments would still be thermally protected by shared thermal energy and could successfully operate at encounter. In addition, the louvers would readjust to account for the change in total power.

The IRS, which requires fairly low temperatures (a target temperature of −36°F for the monochromator), was excluded from the blanket to provide good dissipation to space. Temperature control for the IRS is achieved passively using optical coatings. The exterior metallic surfaces of the IRS are polished with the exception of the radiator and a 26-in.^{2} rectangle on the monochromator, both of which are painted white. Two more heaters are located within the monochromator; one is permanently on and the other is a replacement for the instrument power prior to encounter.

The insulating blanket around the four instruments on the platform is made up by alternating eight layers of nylon netting with seven layers of ½ mil mylar that is aluminized on both sides and sandwiched between an inner and outer layer of 1-mil teflon aluminized on one side (teflon side exposed). The teflon provides a tough, cleanable, and nonconductive surface in contact with the interior instruments. It also provides a low solar absorptivity/emissivity on the exterior of the blanket that will remain cool if sunlit, for example, during separation. Figure 4 shows the platform blanket installed in the flight configuration.

The louver array mounted to the UVS is a half set of a standard array utilized on the spacecraft bus. The surface of the UVS directly beneath the louvers is painted white (PV-100) to provide high emittance when the louvers are in the open position. White is used for low solar

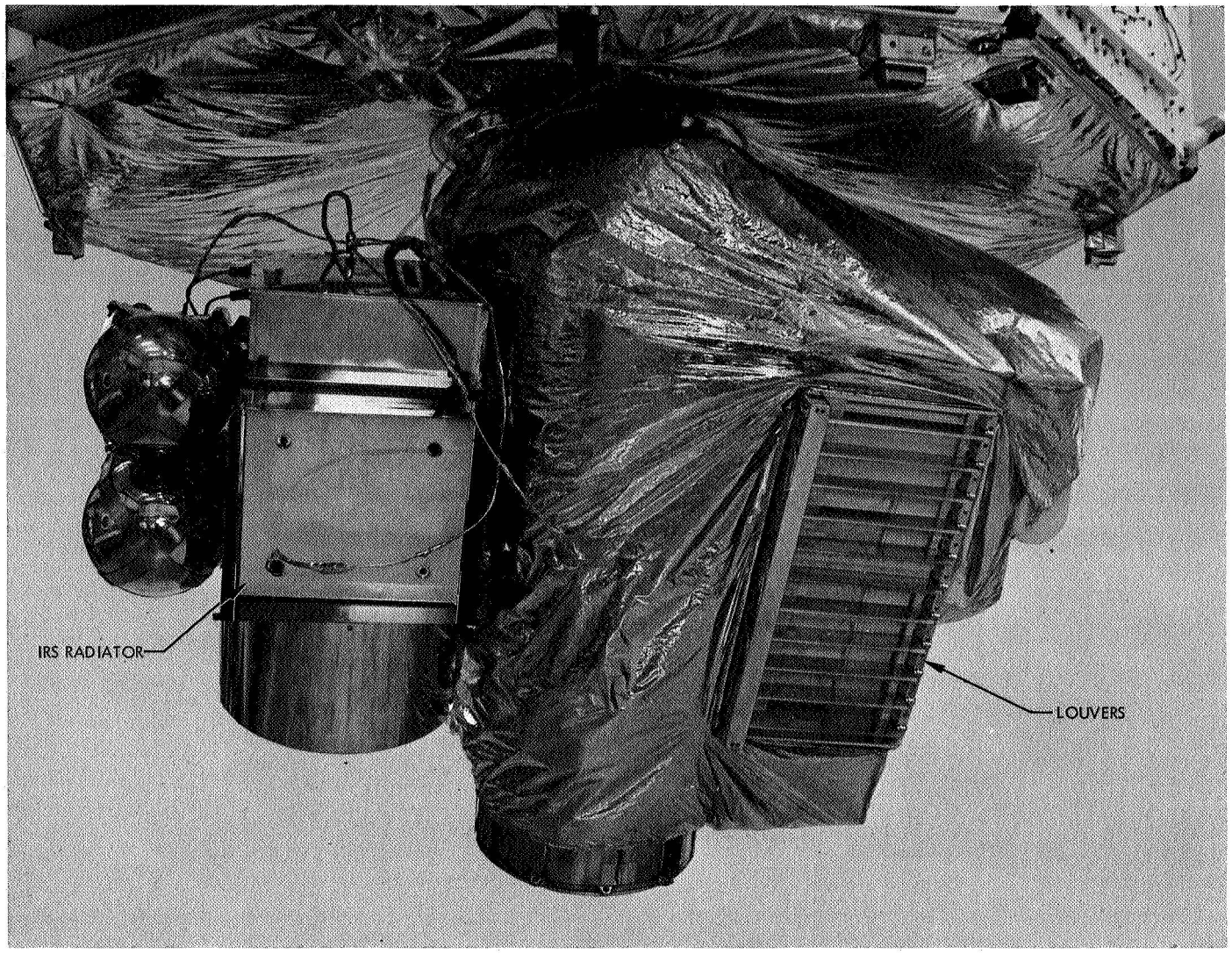

Fig. 4. Platform blanket installed in flight configuration

absorptance to prevent the UVS from overheating if it becomes sunlit during nonsun oriented mission phases.

To prevent excessive loss of heat, exposed metallic portions of the blanketed instrument (aperture assemblies) are polished for low emittance with the exception of the UVS and the IRR. The IRR is, as mentioned, painted white for high emittance since its upper temperature limit is somewhat lower than the other blanketed items.

To decrease heat loss from the telescope optics of TV-B, which has an 8.5-in. diam quartz lens at the aperture, a low IR emittance, high-visible transmissivity coating, developed by Libby Owen Ford, is used on the lens surface. In addition, the TV-B telescope has a wire-wound band heater near the aperture sized to limit gradients along its barrel to less than 4°F so as to prevent thermal distortion.

A diagram of the platform heater and switching circuitry is shown in Fig. 5. The replacement heaters in each instrument and the actuator motor receive their power from the regulated 50 V, 2.4 kHz spacecraft supply. The science instrument replacement heaters are on during the entire mission except encounter. The IRR and actuator motor heaters and louvers are exceptions; they are off during both encounter and recorded science data playback. These heaters are switched through the data storage subsystem relay, which is on during encounter and playback. All other replacement heaters

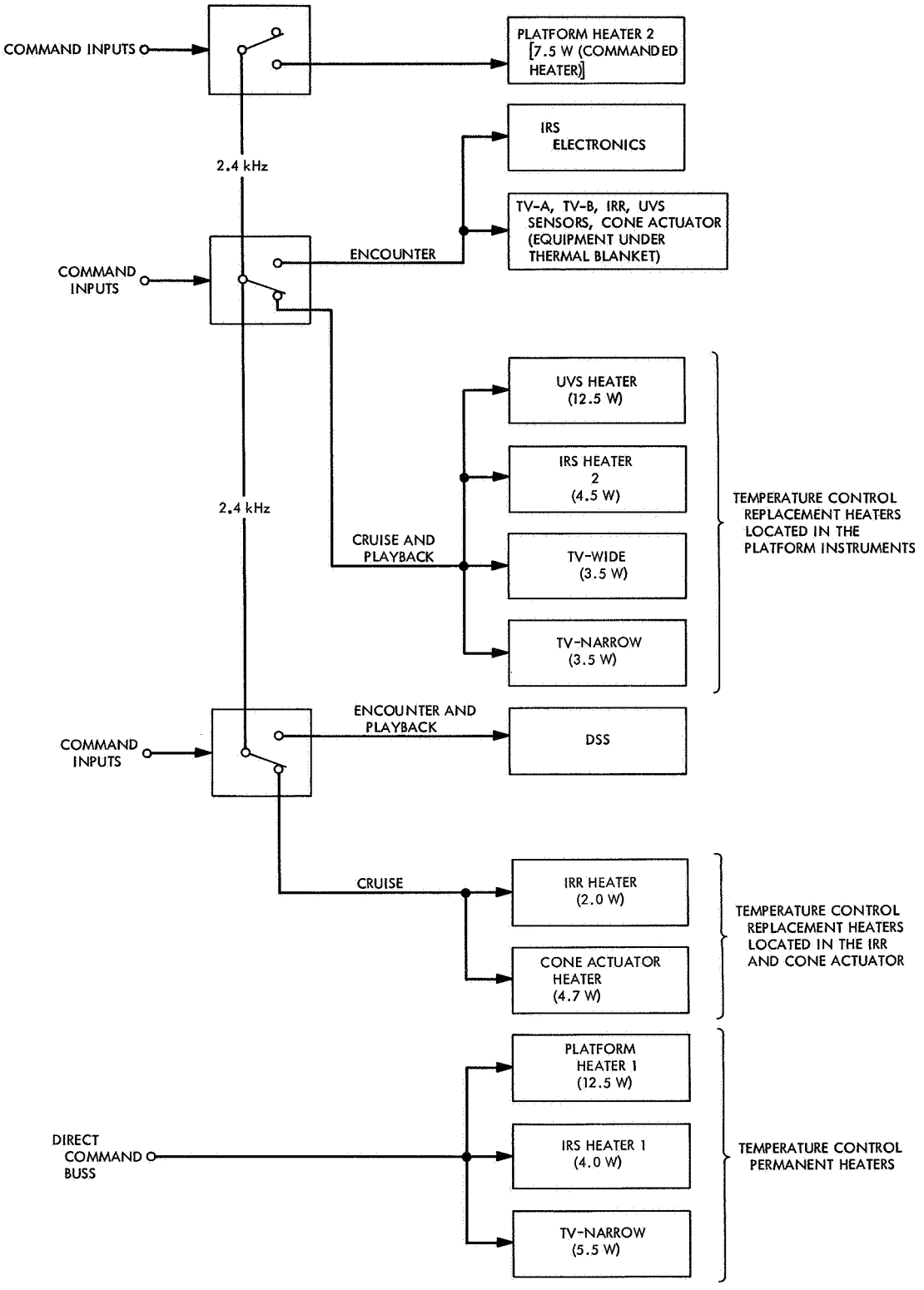

Fig. 5. Platform heater and switching circuitry

are switched by the science on–off relay. The commandable back-up heater, platform heater 2, also operates off the 50 V, 2.4 kHz power supply.

The permanent heaters (platform heater 1, IRS heater 1, and the TV-B optics band heater) are operated off the spacecraft dc bus. The dc-powered heaters, of fixed resistance, have the disadvantage of uncertain voltage and, thus, uncertain power dissipation. The uncertainty in dc voltage results from uncertainty in solar panel (dc source) temperatures and degree of space-induced degradation. The maximum voltage variation is expected to be from a minimum of 36 V at earth to a maximum of 45.5 V at Mars (nominal 43.5 V at Mars). It would have been desirable to have all heaters operate off of regulated ac power, but this would have overloaded the power inverter. Tables 6 and 7 list the power dissipation of platform items for major mission phases.

All heaters used in the temperature control subsystem, except the TV-B band heater, are wire-wound resistors selected from the JPL preferred parts list. The TV-B optics band heater is built of resistance wire embedded in silicon rubber. This heater is approximately 0.10 × 2 × 31.25 in. All heaters are rated for 100% overload.

Test results. The planetary platform design has been tested on the thermal control model, proof test model, and three flight spacecraft. In order to illustrate how the platform temperatures vary with power in the blanketed area, a plot of typical test data from the planetary platform test is shown in Fig. 6. Note the slope of the average instrument temperature for louvers closed, partially open, and fully opened. These three slopes represent average instrument temperature sensitivity to power and the values are 3.0°F/W with platform louvers closed, 1.0°F/W with louvers partially open, and 2.0°F/W for the louvers fully opened. This varying temperature sensitivity is the effect of the louvers changing the effective emittance of the platform and is similar to the response of the louvered spacecraft bus.

Individual instrument temperatures are plotted in Fig. 7 from M69-3 (typical of the three flight units) thermal-vacuum test data. The curve shows that the individual instruments do not have temperature-to-power sensitivity curves exactly alike. The power ranges and number of test data points available from flight test data do not define completely the three distinct slopes as in Fig. 6; however, the trends are typical of louver-controlled devices. The instruments, or portions of instruments, follow the typical louver temperature-to-power curve to the extent that they are radiatively and/or conductively slaved to the louvers.

The temperature control margins are depicted in Fig. 7 by the range on the high and low side of the expected range of power during flight. The temperature control design margin may be defined in terms of a power margin, that is, how much of a power loss will cause any one of the instruments to exceed their required temperature limits. Considering first the low-power margin under the blanket, 6½ W near earth or 12 W near Mars would have to be lost before the IRR would be below its lower limit of −4.0°F. All other blanketed instruments have much wider margins. The low-power margin at encounter power level would be 16 W for the same occurrence. These margins in power can be increased by an additional 7.5 W if the back-up heater is commanded on.

On the high side, the power margin must be in excess of 16 W in the platform before the IRR exceeds the 32°F higher limit of temperature. All other instruments have much wider margins on the high side.

The design margins on the IRS may be derived in terms of the instrument's temperature sensitivity-to-power ratio. The 26-in.^{2} white-painted area on this highly-polished instrument result in a temperature sensitivity-to-power ratio of 3.5°F/W.

The IRS monochromator temperature at encounter for the flight articles during thermal-vacuum testing were −31°F, −28°F, and −30°F for flight spacecraft M69-2, -3, and -4, respectively. If these temperatures are adjusted to account for space simulator chamber effects and the effects of the solar simulator lamps being on during these tests, a value of −35°F can be deduced as a flight prediction. This temperature is 1°F less than the optimal flight temperature for the monochromator. The temperature limit range for cruise conditions, when the instrument is not on, is much wider than for those at encounter.

In order to exceed its *lower* temperature limit of −54°F at encounter, the IRS would have to lose 5.42 W of internal power (the low-power margin), and, to exceed the *upper* limit of −27°F at encounter, gain an additional 2.27 W of power (the high-power margin). These margins should be reduced by the uncertainty in dc heater power, which is ±0.4 W from the nominal 4.0 W near Mars.

Table 6. Power dissipation of planetary platform equipment enclosed by the thermal blanket

Equipment	Power dissipation, W							
	Earth cruise (heaters on)		Mars cruise (heaters on)		Far and near encounter		Playback (heaters on)	
	ac	dc	ac	dc	Instrument ac	Temperature control dc	ac	dc
IRR	2.0	—	2.0	—	2.5	—	0	—
TV-A	3.5	—	3.5	—	3.5	—	3.5	—
TV-B	3.5	3.77[b]	3.5	5.5[c]	3.5	5.5[c]	3.5	5.0[c]
UVS	12.5	—	12.5	—	14.5	—	12.5	—
Cone actuator	4.67	—	4.67	—	5.0	—	0	—
Planet sensor(s)	0	—	0	—	1.0	—	0	—
Platform heater 1[a]	0	8.56[b]	0	12.5[c]	0	12.5[c]	0	12.5[c]
Subtotals	26.17	12.33	26.17	18.0[c]	30.0	18.0[c]	19.5	18.0
Total ac and dc power	38.5		44.17		48		37.5	

[a]Platform heater 2 can provide additional 7.5 W (on command DC-34).

[b]Minimum dc voltage expected near earth is 36.0 V.

[c]Nominal dc voltage expected near Mars is 43.5 V.

Table 7. Power dissipation of planetary platform equipment not enclosed by the thermal blanket

Equipment	Power dissipation, W							
	Earth cruise (heaters on)		Mars cruise and playback (heaters on)		Far encounter		Near encounter	
	ac	dc	ac	dc	Instrument ac	Temperature control dc	Instrument ac	Temperature control dc
IRS								
Monochromator	4.5	2.8[a]	4.5	4.0[b]	3.6 (1st h) 2.5–3.6	4.0[b]	5.6–7.6	4.0[b]
Radiator	—	—	—	—	—	—	—	—
Cryostat gas bottles	—	—	—	—	—	—	—	—
Total ac and dc power	7.3		8.5		6.5–7.6		9.6–11.6	

[a]Minimum dc voltage expected near earth is 36.0V.

[b]Nominal dc voltage expected near Mars is 43.5 V.

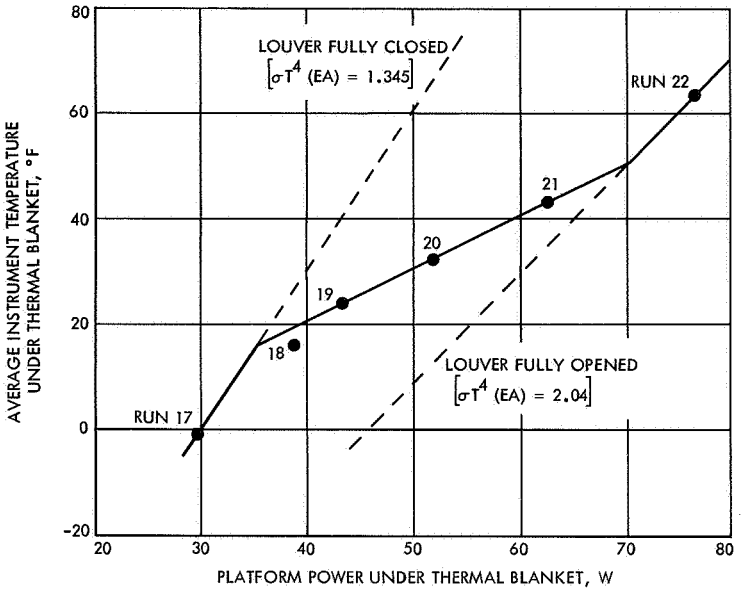

Fig. 6. Performance of scan platform louvers

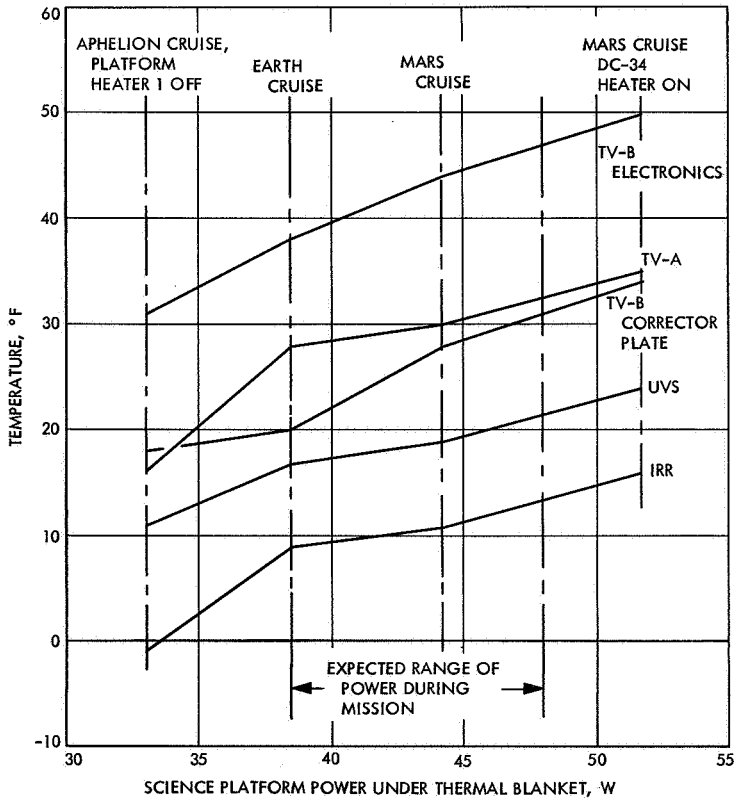

Fig. 7. Platform instrument temperature versus power in the blanketed volume

The temperatures of the planetary platform instruments for major phases of the M69-3 (typical) spacecraft mission are shown in Table 8. All temperatures shown are as measured by thermocouples mounted on the instruments. These measurements and flight-telemetered data from other *Mariner* missions agree to within a few degrees Fahrenheit. All temperatures are within ranges required for the instruments, sensors, and the cone actuator. The TV-B optics gradient was also within the required limits.

The IRS radiator, and hence the channel 2 detector, does not attain the required −171–−189°F temperature. Adjusted chamber data predicts a low of −160°F in flight. The experiment is reported to still operate satisfactorily at this temperature with only a small loss in detector sensitivity.

Special problems. The platform temperature control design is not completely problem free. One problem results from the possibility of facing the science instruments optical axes into the sunlight during the mission. The midcourse maneuvers have been restricted to avoid this possibility, although it still exists during separation and sun acquisition. The TV-B is the most sensitive instrument to sunlight impingement. Even for the short time it takes the sun to pass the TV-B field-of-view at the lowest expected separation rates, the TV shutter would be exposed to a focused thermal heat input that could cause permanent damage to the shutter blade. Calculations place the probability of the sun entering the TV-B field-of-view at approximately 1 in 10,000.

A second problem involves the IRS experiment as it approaches Mars. The predicted planetary radiation and albedo (reflected solar radiation) from the planet impinging on the IRS radiator will be sufficient to raise its temperature approximately 8°F. This increase in temperature occurs at a time when the instrument is taking data and will affect the performance of both IRS data channels. The principal consequence of this variable temperature will be to make IRS data reduction more involved.

2. Scan Platform Structure

a. Introduction. The discussion in *Subsection 1* considers the scan platform from a temperature control point of view. In contrast, this subsection will consider the same platform as a two-degree-of-freedom gimballed support structure upon which the scan actuators and the planet-oriented science instruments and sensors are mounted. The platform structure (Fig. 8) supplies the articulation and the precise mountings necessary to permit the scan subsystem to acquire and track the planet Mars, and for the science instruments to perform the encounter measurements. The scan platform can be divided into three basic areas: (1) the gimbal, (2) the instrument frame, and (3) the latch. This subsection discusses the gimbal and the instrument frame. *Subsection 3* discusses the scan platform latch assembly.

Table 8. Planetary platform instrument temperature test data[a]

Equipment	Earth cruise	Mars cruise	Encounter	Playback	Aphelion cruise
IRR	7	11	17	−2	11
TV-A	25	30	31	22	30
UVS	17	19	22	16	21
TV-B	36	44	44	39	46
TV-B Optics Gradient[b]	2	2	2	0	−1
IRS monochromator	−27	−22	−28	−24	−19
IRS cryostat gas bottles	−34	−36	−30	−34	−31
IRS radiator	−136	−143	−141	−144	−145
Planet sensor and Mars gates	12	19	21	14	23
Cone actuator	28	34	35	19	36

[a]The temperature values listed are in degrees Fahrenheit.

[b]Gradient is positive for a corrector plate warmer than the primary mirror.

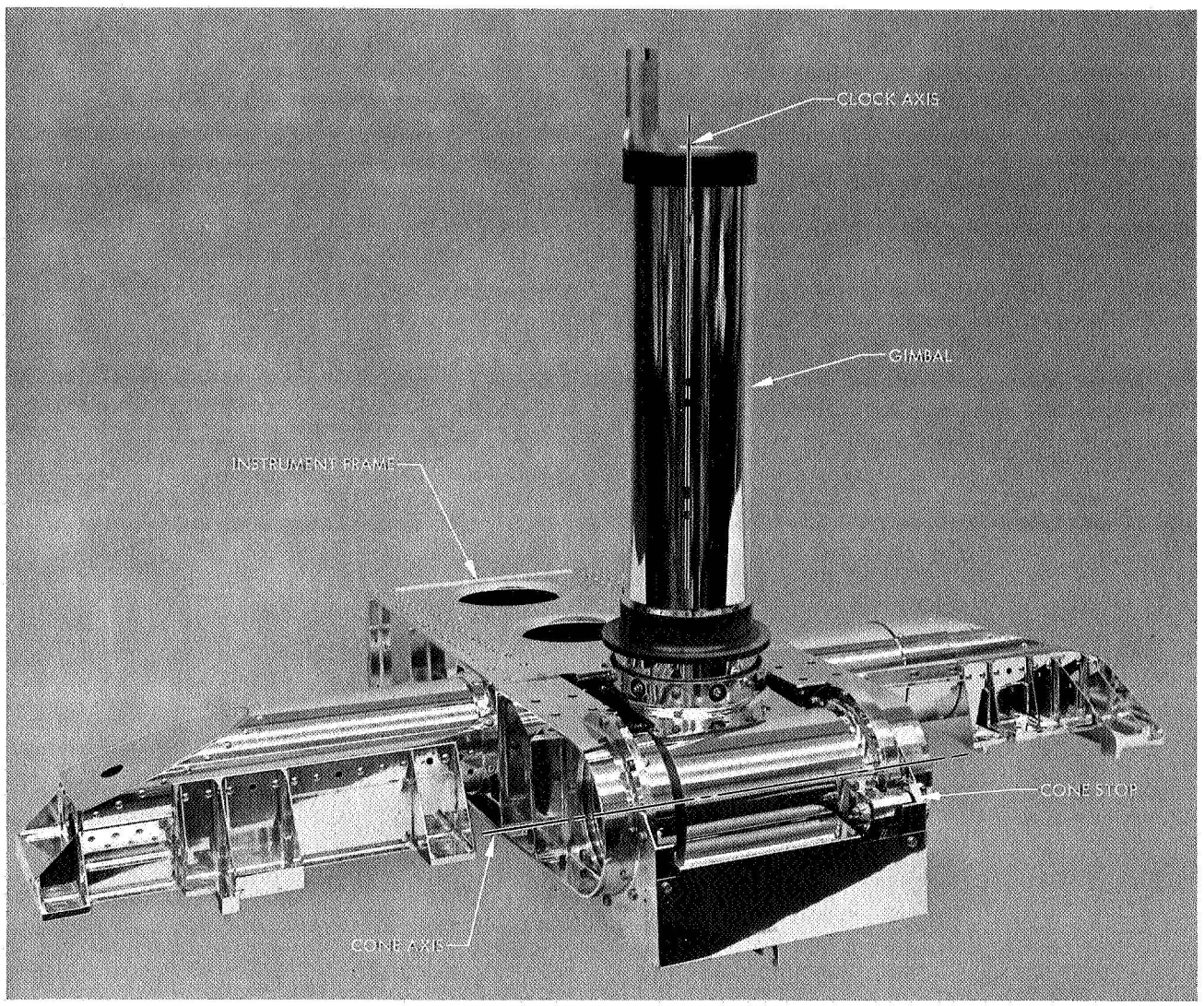

Fig. 8. Scan platform structure

b. Design criteria. The mission requires the platform to be pointable anywhere within the range of an 101–165-deg cone angle, where 0 deg is the spacecraft–sun vector, and a 90–305-deg clock angle, where 0 deg is the center of Bay VIII. The platform was allocated 0.1 deg of the 0.3-deg total instrument and sensor look direction offset permitted from the nominal specified.

The elements of the scan subsystem mounted on the scan platform are:

(1) Clock and cone scan actuators.

(2) Far-encounter planet sensor (FEPS).

(3) Two narrow-angle Mars gates (NAMG).

The science instruments mounted on the platform are:

(1) Ultraviolet spectrometer (UVS).

(2) Wide-angle television camera (TV-A).

(3) Narrow-angle television camera (TV-B).

(4) Infrared spectrometer (IRS):

  (a) Monochromator–telescope.

  (b) Gas bottles.

  (c) IRS gas disposal system (IRS vent).

(5) Infrared radiometer (IRR).

The weight of all sensors, the cone actuator, and the science instruments that move with the platform is approximately 122 lb. This does not include the clock actuator since it is mounted on the bus. Some of the sensors and instruments require thermal and/or electrical isolation from the platform.

In addition to the above sensors and instruments, two heaters, an accelerometer, and an alignment mirror are mounted on the platform. A cable harness for power, pyro, accelerometer, and science signals must be routed from the bus cable trough, through the two axes of articulation, to the items mounted on the platform. The torques seen by the scan subsystem during space flight must be less than 40 in.-lb to give acceptable scan subsystem pointing direction offsets.

The spacecraft configuration dictated the platform location underneath the bus. In the launch configuration, the platform extends down into the spacecraft adapter. Upon spacecraft separation, the platform must have adequate clearance to exit from the adapter. The available envelope within the adapter dictated a 96-deg stowed cone angle.

The platform design is based upon locking the platform to the bus during the launch phases to directly transfer the launch loads to the bus. Upon platform latch

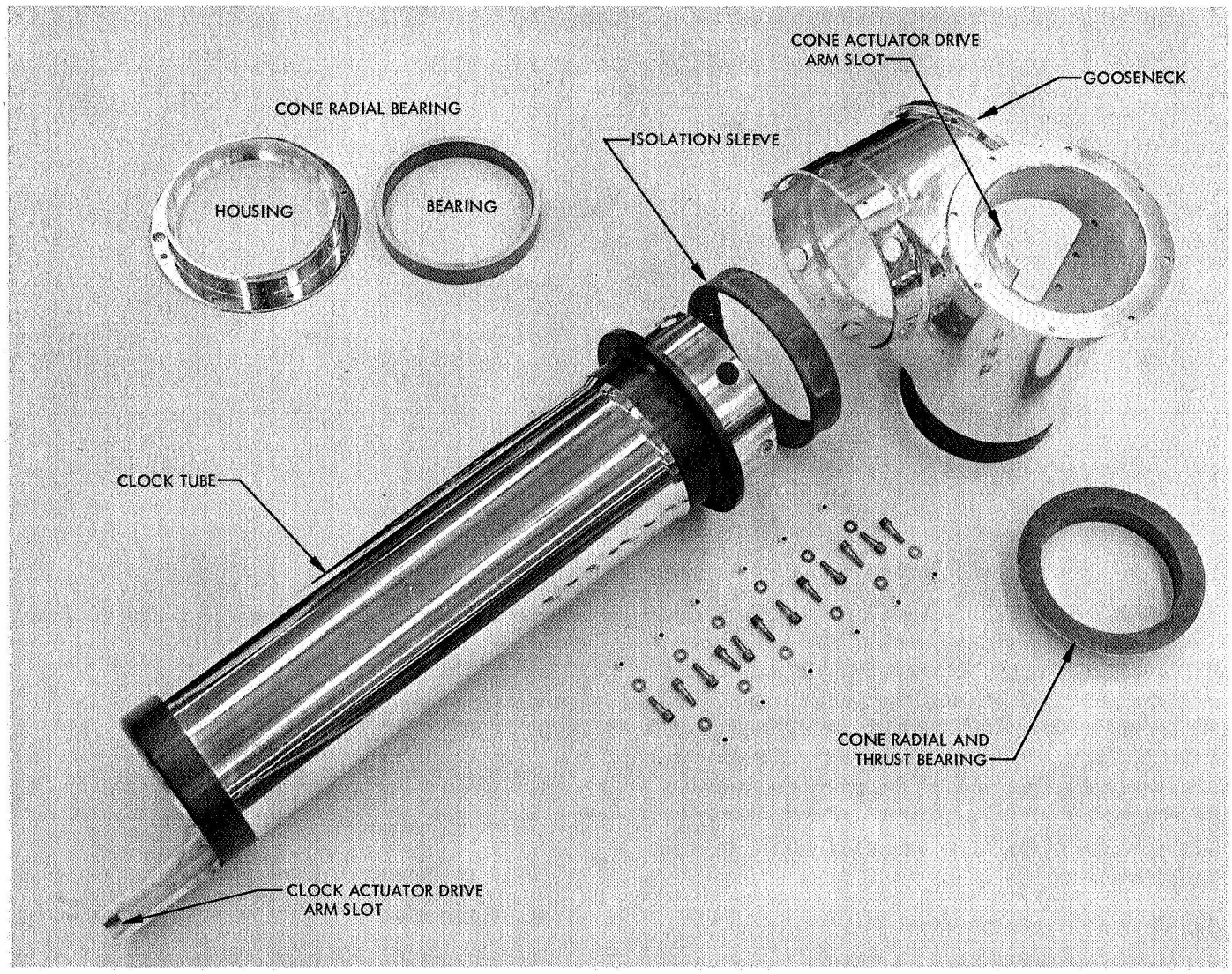

Fig. 9. Scan platform gimbal

release, the restraint is slowly removed and the entire platform translates 0.060 in. along the clock axis in the z-axis direction. Once released, the platform is attached to the bus through the gimbal only.

c. Description. The gimbal provides both clock- and cone-angle articulation. The platform clock axis coincides with the spacecraft z axis. The gimbal is made of three primary pieces: (1) the clock tube, (2) isolation sleeve, and (3) clock–cone adapter (gooseneck). The clock tube passes through two sleeve bearings in a tube in the bus and is restrained by a thrust bearing acting on a flange on the clock tube. The upper half of the thrust bearing is spring loaded to permit the 0.060-in. axial movement when the platform is latched. The clock actuator is mounted on an adapter on the bus upper ring and drives the clock tube by an arm that rides in a slot in a tongue in the tube.

The scan platform gimbal is shown in Fig. 9. The clock tube fits into the fiberglass isolation sleeve, which fits into the gooseneck. A combination radial and thrust bearing is pressed into one end of the gooseneck and the outside diameter (OD) of the gooseneck at the opposite end serves as the shaft of the other cone radial sleeve bearing. This latter bearing is fastened to the instrument frame, as is the cone axis bearing adapter which fits into the combination radial and thrust bearing. The cone actuator is mounted on the instrument frame and drives the platform through a drive arm which fits into a slot in a bracket riveted into the gooseneck.

The bearings are a nominal 0.014-in. layer of a teflon-filled asbestos matrix bonded on aluminum. The bearing material was chosen for low friction, stability, and reliability in a space environment. The bearings run on hard anodized aluminum surfaces.

The instrument frame (Fig. 10) is a box section with a tube passing transversely through the center. This configuration was chosen to permit rapid recovery from any design changes in instrument or sensor look directions. The primary instrument, TV-B, to which all other instrument and sensor look directions are referenced, is located on the box section. The other instruments are mounted on

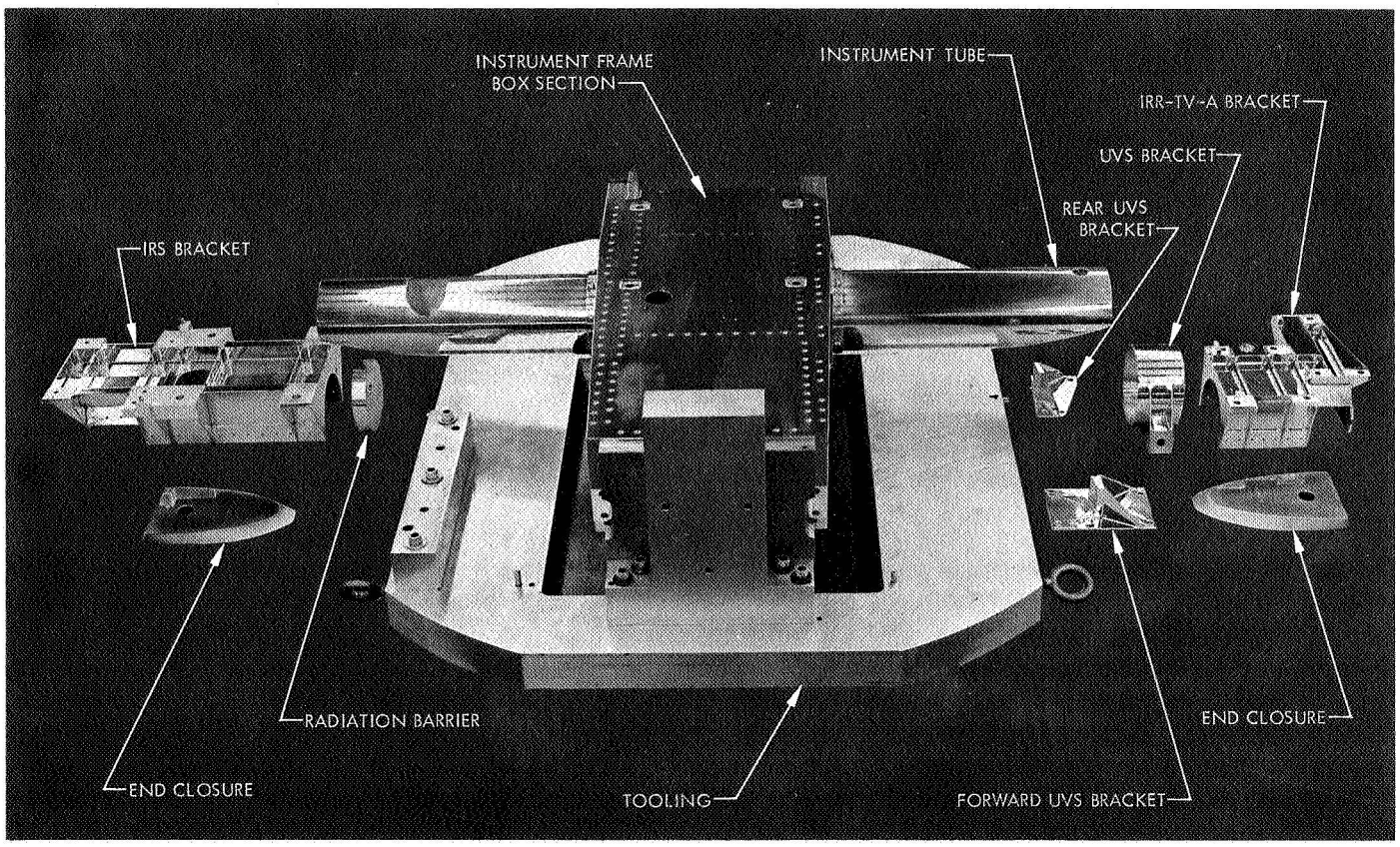

Fig. 10. Instrument frame box section with instrument tube and brackets

brackets fastened to the tube. The box section is composed of two side beams and an outboard beam, all of which are machined, and two sheet-metal surface skins and two sheet-metal transverse webs. The instrument tube has a 4-in. diameter with 1/8-in. walls in the center third and 1/16-in. walls at the outboard ends. The brackets mounted on the tube are designed to rely minimally upon the instrument tube for support. The result is a stronger assembly with the brackets and tube reinforcing each other.

The top side of the ends of the instrument tube are relieved, or beveled, at 18 deg to provide clearance to the lower thermal shield. To maintain tube rigidity at the ends, these large cutouts are bridged by end closures.

The instrument mounting and alignment surfaces are shown in Fig. 11. As has been mentioned, TV-B mounts on the bottom of the instrument frame box section. The instrument is electrically isolated from the platform by four hard anodized aluminum washers, with the bolts isolated by fiberglass shoulder bushings. The TV-B is aligned on the platform by pushing fiberglass pads on the rear of the instrument against two dowel pins. In the inspection of the instrument and sensor mounting planes and angles, all measurements are referenced to the area established by three of the TV-B isolation washers and to a line tangent to the two dowel pins.

The IRS is located on a bracket on the instrument tube, with the monochromator–telescope adjacent to TV-B and the gas bottles on the outboard end. The monochromator–telescope is electrically and thermally isolated from the platform by hardware provided by the experimenter. Because the IRS requires a much colder operating temperature than the other instruments, great effort was taken to reduce heat flow to the instrument. The IRS is positioned on the platform by setting the distance from the side of the instrument to two platform dowel pins. This 0.100-in. spacing prevents heat flow into the instrument. The IRS cryostat protrudes from the instrument beyond the mounting plane, which results in a

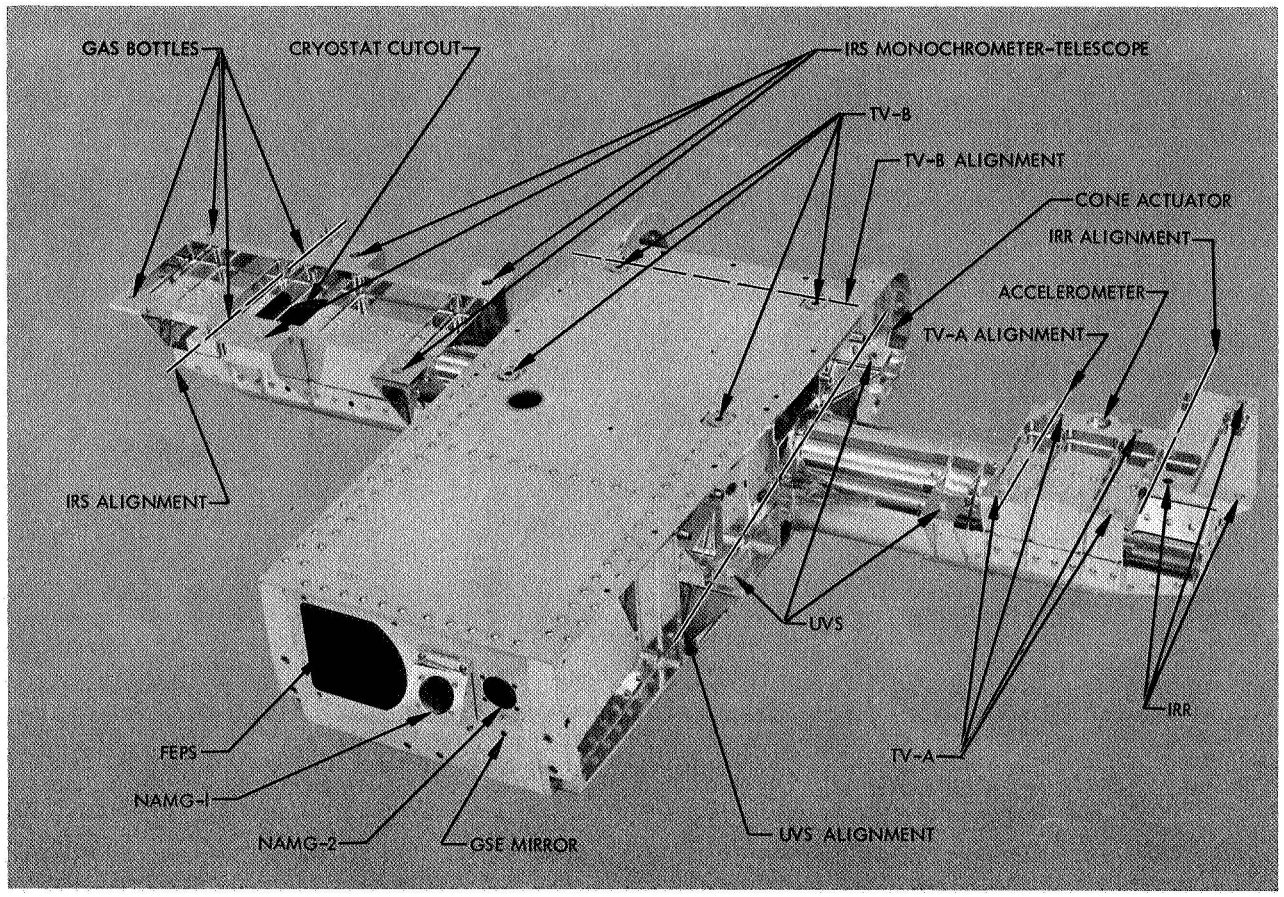

Fig. 11. Instrument and sensor mounting points

2.00 × 2.81-in. hole through the IRS bracket and into the instrument tube. To prevent the cryostat from seeing the warm end of the instrument tube, a radiation barrier is installed inside the tube approximately where the tube enters the box section. The gas-bottle assembly is bolted directly to the platform, with the position set only by the four mounting bolts.

The IRS vent is a 1/2-in.-diam tube inside the instrument tube parallel to the cone axis. The vent tube is rigidly mounted at two central points and restrained at the ends at the free state position. This vent configuration was chosen to permit installation of a completely aligned and pretested unit rather than simply bolting on two nozzles and plumbing and later worrying about thrust axis alignment and balanced thrusts.

The UVS is mounted on the side of TV-B opposite the IRS. The forward and aft feet sit on brackets bolted to the left beam of the box section and are pushed against two dowel pins for alignment. The third UVS foot sits on a bracket on the instrument tube. Since no electrical or thermal isolation is required, the UVS is bolted directly to the platform.

The TV-A and IRR are mounted outboard of the UVS. The IRR is set back from the TV-A to provide clearance to an umbilical island in the adapter. Both instruments are aligned by pushing them against two shoulders on the mounting bracket. Both the IRR and TV-A are electrically isolated from the platform. The TV-A has fiberglass pads against the alignment shoulders, sits on a fiberglass washer, and has the bolts isolated by fiberglass shoulder bushings. The IRR mounting isolation is similar to the TV-A except that the fiberglass at the alignment interface is on the platform shoulders.

The FEPS mounts inside the box section looking forward through the outboard beam. Alignment is given by two shoulders. The NAMG's are mounted on the front of the outboard beam, with alignment accomplished from just the bolt pattern. The NAMG-1, which starts IRS cool down, is mounted on a wedged block which, in turn, is bolted to the outboard beam. The NAMG-2, which initiates the near encounter sequence, bolts directly to the outboard beam. A mirror, used during alignment measurements, bolts to the outboard beam and is rotationally constrained by a dowel pin.

The platform flight accelerometer is mounted on the IRR–TV-A bracket by the rear of TV-A. Two thermal-control heaters are mounted on the left beam and a temperature transducer is located in the gimbal gooseneck.

The two scan actuators fit into shallow, close-tolerance bores and are located at a specified angle by dowel pins.

The routing and support of cabling from the bus to the platform presented a difficult problem. The original intent was to separate power, pyro, signal, and scan wires into four bundles to reduce crosstalk and noise in the signal lines. For simplicity, and to reduce torque required to turn the cable bundle, the harness through the gimbal is a loose single bundle that flares between mounting points to prevent crosstalk. The cable harness gathers from various points on the bus at the port in the clock actuator adapter. The harness then makes a 90-deg bend to align with the clock tube and passes through the interior of the tube down to the gooseneck. In the gooseneck, the bundle makes two 90-deg turns to the cone axis and exits at the rear of the IRS. From this point, the harness spreads outward to the instruments, sensors, heaters, accelerometer, and cone actuator. The movement of the gimbal axes is accommodated in the harness by torsion rather than bending. The harness is tied to the bus and to the gooseneck at the top and bottom of the clock tube, respectively, with a combination bumper-guide in the center. The harness is fixed with respect to the cone axis in the gooseneck and moves in cone with the platform at the exit from the gooseneck. Attach points and supports are placed at intervals along the platform to restrain the cabling.

Thermal-control considerations resulted in polished external surfaces to reduce heat losses, black paint on the interior of the box section to increase internal heat transfer, the radiation barrier inside the instrument tube, the isolation sleeve in the gimbal to reduce heat flow between the bus and platform, and nylon hook and pile fasteners bonded on exterior surfaces for attaching thermal shields.

As described before, the platform instrument frame is tied to the bus during launch. After the first midcourse maneuver, the platform restraint is removed by a pneumatic latch mechanism described in *Subsection* 3. As the platform releases, it moves away from the bus along the clock axis 0.060 in. The spring-loaded thrust washer follows this movement until the outer edge of the thrust washer sets against the clock axis split-cap bearing. The platform movement remaining after the thrust bearing seats provides the thrust axial clearance necessary for

smooth operation. The rotational movement of the platform is constrained to the specified operational envelope by mechanical stops. The location of the two clock stops is fairly critical because the actuator position potentiometers become unstable approximately 1 deg beyond the stops. The cone axis stop has a dual range. The platform is stowed at a cone angle of 96 deg. The stop is set slightly below this angle to prevent the platform from coming up into the bus, and the platform is able to slew the entire clock range at a cone angle of 96 deg without striking the bus. However, the platform operational cone envelope is 101–165 deg. Therefore, when the platform cone angle passes 101 deg, the cone stop pin drops off a shelf into a slot with cone limits of 101–165 deg and the platform is prevented from returning to the stowed position until the pin is retracted manually.

d. Testing. After installation in the bus, the platform structure is tested for smooth and low-torque operation using a mockup actuator and a dial torque wrench. During systems tests of the scan subsystem, the platform is driven by the actuators and the operation is noted. Each flight unit is operated, although through small movements, in the space simulator. The thermal qualification of the platform was done during the TCM tests, both in separate platform thermal studies and on the bus in the JPL 10-ft space simulator. The platform was subjected to proof loads without damage during design test model (DTM) vibration testing. It was found that the accelerations were one-half of the predicted levels. The platform was type-approval qualified on the proof test model (PTM) during the PTM vibration and thermal testing. Similarly, flight acceptance qualification was accomplished on the flight spacecraft during vibration and space simulator testing.

e. Problems. After extensive systems, vibration, and space simulator testing, it was found that the PTM platform had tilted with respect to the bus. Examination showed that the box section was undamaged and, therefore, all distortion was in the gimbal. Although the bolts joining the clock tube and thermal isolator were found to have enlarged their holes, this did not account for the tilt. Since the gimbal was found to be relatively weak when an access cover is removed, it was surmised that the damage occurred during a period of systems testing when the cover was not installed. As a result of finding that the cover provides structural support, and is not merely protective in nature, its thickness was increased from 0.020 to 0.063 in. Also, it has been specified that the cover be in place during testing. The elongation of the bolt holes in the fiberglass isolation sleeve was traced to testing in the Spacecraft Assembly Facility (SAF); M69-3 was undamaged both prior to and after vibration, and the DTM was much less damaged than the PTM although experiencing much higher vibration levels. It was found that the platform can impose 2100 in.-lb of torque across the isolator joint in one system test configuration. The solution was to install bushings to increase the bearing area and to warn test personnel of the possibility of damage during exuberant testing.

During testing, the running torque of the PTM platform in clock angle was found to be excessive. The problem was traced to a distortion of the thrust bearing causing it to drag on the clock tube flange. This problem was solved by increasing the shim thickness to give adequate thrust bearing clearances.

The platform cone angle range capabilities in the loaded configuration in a 1-*g* field are lower than expected. It was found that the actuator slip torque, combined with the frictional load due to gravity and actuator arm thrusts, gives very limited ground test cone angle capability (on the order of 10 deg on either side of the neutral rest position in the 1-*g* field).

3. Scan Platform Latch Assembly

a. Introduction. The scan platform is latched to the main equipment compartment during the launch and first maneuver periods to (1) minimize the design loads for the structure members and drive mechanisms, and (2) to assure a minimum of dynamic interaction between the platform structure and the autopilot during the trajectory correction maneuver. The second maneuver, if required, is expected to be of such a short duration that this latter effect would be negligible. A simpler latch could have been devised, but a sudden release of the strain energy stored in the flexible structure of the platform would have subjected the science instruments to an unnecessary shock. It was not known during the early design phase of the project whether or not this shock would have been damaging to the instruments; however, it was decided that it would be better to avoid this problem at the expense of a more complex latching technique.

To minimize the effect of the residual strain energy, two general design criteria were set forth. First, the platform would be attached as directly to the main structure as possible, paralleling, if possible, any secondary structure, bearings, or actuators. Second, the platform release

would be such that any unavoidable strain energy would be released slowly.

b. Design. The design criteria mentioned above resulted in a design which holds the scan platform in its stowed, or launch, position by means of four pneumatic latch mechanisms manifolded together to obtain parallel release. The latch points are located approximately at the four corners of the basic box structure of the platform, thus forming a broad base for load transfer to the bus structure. Latch preload is applied by pressurizing the manifold to engage T-bar latches at a serrated interface as illustrated in Fig. 12. Piston areas were chosen to give preloads of approximately 5700 lb at each inboard location and 1600 lb at the outboard latches when pressurized to 1500 psi. This preload, in conjunction with the serrations, ensure no joint separation or slippage within the design loads expected at the platform.

Platform latch release is initiated by firing a normally-closed pyrotechnic valve to allow manifold venting to space. To minimize the resultant torque reaction on the spacecraft, venting is accomplished through a sintered plug restrictor to limit flow rate and is discharged overboard through a balanced T-fitting. The 4-in.^{3} manifold is vented from 1500 psi to the nominal unlatching pressure of 100 psi in approximately 30–60 s. Piston return springs were sized to allow the outboard latches to disengage slightly before the inboard latches. This was done to ensure that the 0.060-in. z-axis translation of the platform to clear the serrations during release would not cause undesirable torques on the cone axis actuator.

Latch pressure is monitored through spacecraft telemetry as an engineering measurement on the low-low deck. This status measurement was chosen instead of an event indication to allow system test and on-pad monitoring of possible leaks which could cause a launch hold. In addition to pressure, microswitches at each latch are wired in series to give an event indication when all latches have released.

The latch manifolds were built as inboard and outboard subassemblies, installed separately on the spacecraft structure, and connected together with stainless tubing having standard 1/4-in. flare fittings on each end. Manifold cylinders, interconnects, and fittings were fabricated from stainless steel for weldability.

c. Assembly. To ensure leak-tight welds, clean room assembly was performed utilizing techniques developed for the attitude control gas subsystem. These include contamination control, weld fixture assembly, and inert gas purging, as well as radiographic and fluorescent penetrant inspection methods.

Final assembly of pistons and seals was performed on a class 100 clean bench with leak- and proof-pressure tests performed separately on inboard and outboard subassemblies. These two latch manifold subassemblies, plus the interconnect tube and spacecraft-mounted serrated support blocks, form the deliverable, spacecraft installation-level platform latch hardware weighing approximately 13.5 lb.

Installation of the latch hardware onto the bus and platform structures was performed by detailed alignment procedures which compensated for piece-part tolerances at the latch interface. Following initial installation, the latch assembly was regarded as part of the spacecraft structure not requiring further adjustment or removal for maintenance. The mating latch components attached to the platform structure were also allowed to remain in place through the normal platform installation and removal procedures, thus ensuring proper mated alignment.

d. Latch testing. Due to the small (4-in.^{3}) volume of the latch manifold, considerable attention was given to the design and verification of a leak-tight assembly. The requirement to maintain the fill pressure of 1500 psi through an estimated 4 wk of encapsulation and launch environment, in addition to maintaining an in-flight pressure of no less than 1200 psi for the six-month cruise phase, was an early design concern.

To verify the approach, many early tests were performed to select the proper seals, geometry, cleanliness, and required surface finish for the eight dynamic seals and three static seals utilized in the design. These tests were completed successfully with standard Viton O-rings in conjunction with Parker "Parbloc" backup rings for the dynamic seals and standard flare tube connections with copper gaskets for the static seals. No detectable leakage has occurred in any test or flight assembly during any phase of the *Mariner* Mars 1969 program.

To ensure leak-tight weldments at the 12 joints in the assembly, numerous weld samples were prepared to verify an acceptable joint design with radiographic and cutaway sections being inspected for proper penetration and homogeneity of the weld. The joint configuration and welding procedures employed have resulted in a test history of no leakage.

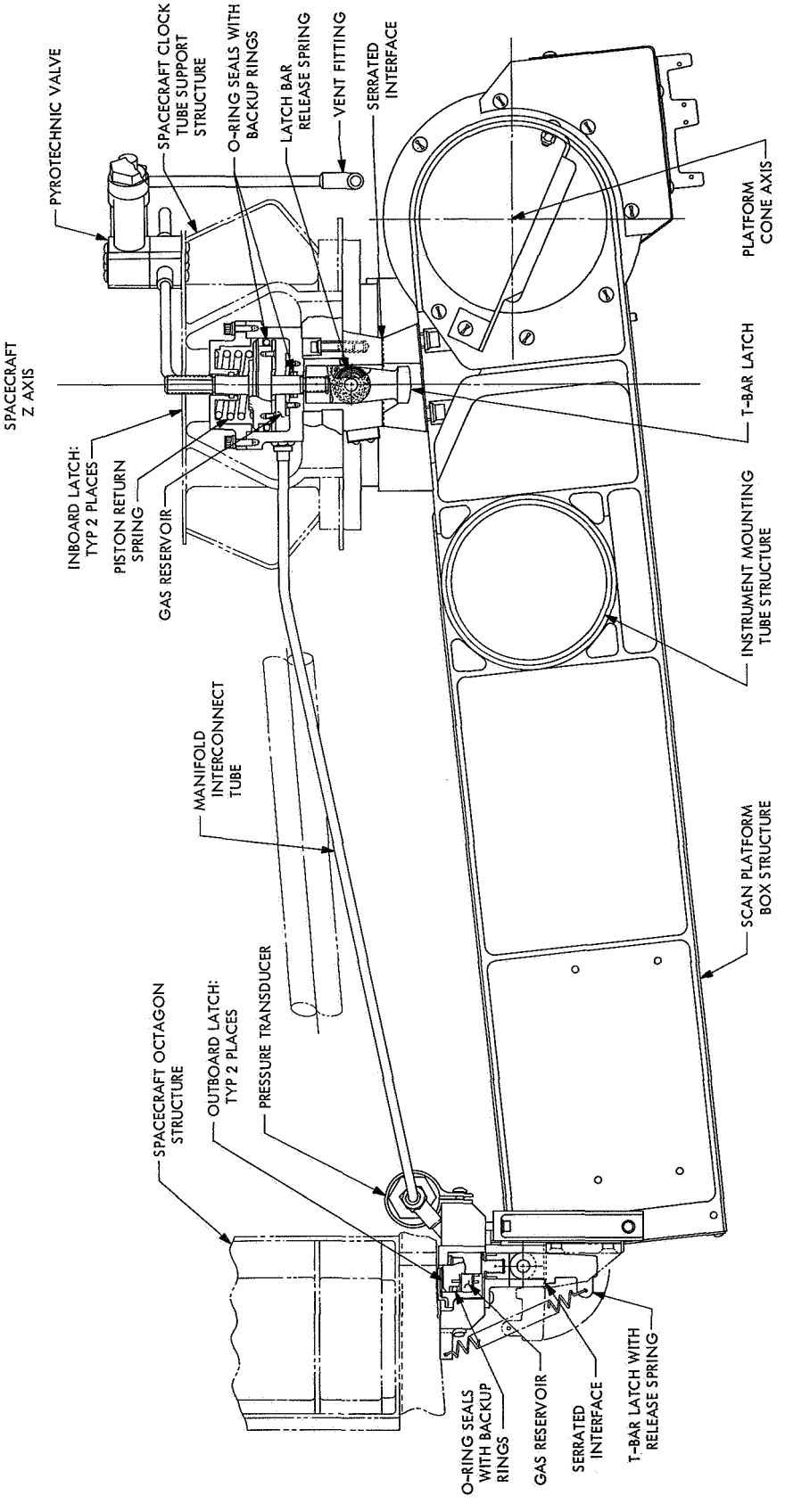

Fig. 12. *Mariner Mars* 1969 scan platform latch installation

Tests on the latch assembly installed on the design test model and flight spacecrafts include vibration and thermal-vacuum qualification at the system level as well as live pyrotechnic valve release tests on each assembly. To date, the only problems noted have been with the post-fire integrity of the pyrotechnic valve which exhibited a tendency to leak following actuation and also to discharge squib debris into the manifold due to blow-by. The former problem was remedied by the addition of electron beam case welding and redesign of the interface gasket. The latter (blow-by), although not eliminated by valve redesign, was minimized to an acceptable level by incorporating prefilters in the manifold vent restrictor. Test results on the modified valve with filters indicate the effect on manifold venting time to be less than a 10% increase due to debris. No debris has been detected downstream of the restrictor filter.

E. Guidance and Control

1. Power Subsystem: Power Profile for Flight Spacecraft

Hard-line power profile measurements obtained from the *Mariner* Mars 1969 proof test model (PTM) spacecraft M69-1 have been described in SPS 37-53, Vol. I, pp. 32–33. Tests are now almost complete for the flight spacecraft, from which power profile data has been obtained solely through the spacecraft telemetry system. Available power profile magnitudes reduced from this data are given in Table 9. The PTM power profile data is presented again for reference, although spacecraft heaters were modified for the flight units. Allocated power profile levels based upon worse-case loadings are also shown.

Power subsystem test data has been obtained in a special ground test in which a *Mariner* Mars 1964 solar array and a *Mariner* Venus 67 battery were the sole power source for the *Mariner* Mars 1969 prototype power conditioning equipment and simulated loads. These tests have indicated that the maximum power point of the solar array (SPS 37-53, Vol. I) at Mars must exceed the steady-state power demand of the spacecraft, with encounter science and high-power TWT loads, by more than 11 W if battery share (SPS 37-52, Vol. I, p. 25) is to be avoided. The worst-case array maximum power point is shown to exceed spacecraft power demands in this operative mode by 42 W for M69-2, 50 W for M69-3, and 47 W for M69-4.

Table 9. Spacecraft steady-state power requirements

Operational modes	Power at the solar array, W				
	M69-1	M69-2	M69-3	M69-4	Allocated
Near earth[a]					
Pre T−200 min	—	267	—	265	—
T−100–T−9 min	—	—	264	280	—
T−9 min to booster separation	284	273	274	270	330
Roll search, near earth	279	267	270	271	320
Maneuver	279	269	271	—	355
Earth cruise, battery charging	253	—	—	—	312
Earth cruise, battery not charging	250	241	243	244	276
Near Mars[b]					
Mars cruise	253	244	248	247	274
Roll search, Mars	280	275	271	279	320
Far encounter	298	283	282	—	353
Near encounter, low TWT	292	292	—	—	349
Near encounter, high TWT	—	332	324	327	389[c]
Playback	288	288	286	290	320

[a]Minimum assured array power near earth is 780 W with no array degradation and 647 W with maximum array degradation.
[b]Minimum assured array power at Mars is 449 W with no array degradation and 374 W with maximum expected radiation degradation.
[c]Array-battery share with 374 W Mars array.

2. Power OSE and its Evolution

a. Introduction. The power operational support equipment (P-OSE) described herein was developed to test the *Mariner* Mars 1969 flight power subsystem (FPS) when in the Case I and Case VIII configurations in the laboratory, at the spacecraft assembly facility (SAF), and at the Air Force Eastern Test Range (AFETR). The P-OSE was originally fabricated for similar testing of the *Mariner* Mars 1964 FPS, modified to test the *Mariner* Venus 67 FPS, and subsequently modified to test the *Mariner* Mars 1969 FPS. This article describes the evolution, design changes, and equipment of the *Mariner* Mars 1969 P-OSE.

b. Evolution of the P-OSE design.

Mariner *Mars 1964 P-OSE.* The P-OSE was designed and newly fabricated to test the *Mariner* Mars 1964 FPS, which consisted of the power conditioning equipment (Cases I and VIII) and the battery. The OSE was designed in three configurations: (1) the laboratory test set (LTS), (2) the system test set (STS), and (3) the launch complex set (LCS).

The LTS is made up of an STS plus a laboratory adapter rack (LAR) (SPS 37-26, Vol. II, pp. 21–23 [confidential]). The LTS was designed to power, control, and monitor the power-conditioning equipment when assembled in its two cases and operating either separately or together. The testing consists of acceptance tests in the contractors' test area, subsystem evaluation tests, flight acceptance (FA) tests, type approval (TA) environmental qualification tests at the environmental test facility, and life tests in the laboratory.

The STS and each assembly was described in SPS 37-21, Vol. II, pp. 20–23 (confidential). This equipment was designed to provide the necessary power, control, and monitoring functions to support the FPS during spacecraft test operations at SAF for initial power application, power subsystem evaluation, and spacecraft system testing. The STS was also used as part of the LTS at the spacecraft environmental test facility.

The LCS was designed to provide the power, control, and monitoring required during launch operations. The LCS consisted of a control panel assembly within the blockhouse, a rack of equipment in the launch pad area, and the ac–dc conditioner mounted in a junction box in the umbilical tower.

Mariner *Venus 67 P-OSE. Mariner* Mars 1964 P-OSE was improved and modified to meet the *Mariner* Venus 67 FPS design requirements. The modifications consisted of the following changes:

(1) The OSE was modified to simulate three-section solar panels instead of the four-section *Mariner* Mars 1964 panels. Also, the simulator calibration was changed to match the characteristics of the new solar panels.

(2) Zener diodes were placed across the OSE external power circuits so that an over-voltage could not be applied to the spacecraft power subsystem.

(3) A one-shot circuit was added to the kinetic switch (controlling transfer from external to internal power) control circuit to ensure sufficient time for the switch to complete its travel. This eliminated the possibility of completing only a partial switch contact transfer by a momentary closure of the transfer control button on the control panel.

(4) The vacuum-fail interlock (for use in environmental testing), which was made inoperative in *Mariner* Mars 1964 was rewired and made to function.

(5) The wire gauge to the kinetic switch was increased within the STS and LCS.

(6) Additional fans were added to the STS and LCS to cool the 400-Hz regulator.

(7) The tolerance detectors were redesigned to reduce temperature effects and drift. One pair of the detectors was substituted in the booster regulator output monitor circuits.

(8) An ac 60-Hz power light was added to the blockhouse power control panel assembly and self-test calibration test points were added to the auxiliary power supply assembly and the self-test assembly.

Mariner *Mars 1969 P-OSE.* The equipment modified for *Mariner* Venus 67 was again modified for *Mariner* Mars 1969. Fund limitations permitted the accomplishment of only about 60% of the changes proposed to update and improve the P-OSE. Briefly, these changes or improvements include the following:

(1) Changing Zener diodes in over-voltage protection circuits to the *Mariner* Mars 1969 voltage levels.

(2) Replacing the tolerance detectors, and their power supplies for the booster regulators, with those having a 60-Vdc maximum sensing level.

(3) Adding several inhibit and interlock circuits to prevent improper and unsafe power subsystem operation.

(4) Adding circuit cards for the 4A17 inverter monitor.

(5) Connecting the A and B portions of the dual power-source/simulator assembly in parallel with diodes.

(6) Adding a 2.4 kHz buffer amplifier in the ac–dc conditioner assembly.

(7) Adding system test computer data system (STCDS) buffer amplifiers and signal conditioning circuits.

(8) Adding a power synchronization free-run test command circuit, a sun-gate command circuit, and a battery-charger test command circuit in the test monitor assembly. Modifying the booster regulator sensing test command circuits, the power distribution test command circuits, and replacing the dummy load resistors where required in the test monitor assembly.

(9) Dividing the LAR control panel into separate control assemblies for Case I and Case VIII, changing the LAR display lights from ac to dc power, replacing all LTS external cables, and adding circuits and test equipment to test the synchronizer oscillator.

(10) Modifying the FPS simulator equipment rack to *Mariner* Mars 1969 OSE requirements.

(11) Modifying the solar panel simulator supplies (dual power-source/simulator assembly) and the solar panel substitution J-boxes for the six-section *Mariner* Mars 1969 solar panel configuration.

(12) Increasing the voltage capability of the kinetic switch power supply.

c. Design changes. Though many design changes and improvements were made to the OSE, generally, these changes were slight and required only moderate modifications. The majority of the changes were required by changes in load levels and voltage levels, addition or deletion of command circuits and monitoring circuits, requirements for more accurate measurements and better buffer amplifiers, and replacement of worn or obsolete equipment. More extensive changes were made in the LAR and the FPS simulator.

Two typical OSE changes that indicate the complexity of the changes were the addition of a frequency counter in the STS to measure the power synchronizer oscillator frequency and the paralleling of OSE power supplies to increase the capability to supply adequate power to the FPS.

The relocation of the spacecraft frequency synchronization oscillator from the *Mariner* Venus 67 central computer and sequencer (CC&S) subsystem to the *Mariner* Mars 1969 power subsystem shifted the requirement for the measurement of this frequency from the CC&S OSE to the P-OSE. This was accomplished with the addition of the digital counter in the P-OSE STS and the interconnections and modifications of all control and test circuits related to the measurements.

The kinetic switch, used to switch the spacecraft from external to internal power, is a make-before-break-type switch that briefly connects the battery and the spacecraft power switch and logic output in parallel. Current limiting was encountered in the external power supply when spacecraft power was switched from internal (battery) to external power. The power switch and logic output voltage dropped from 25–19 V, before going to 40 V, for 0.30 s due to this limiting and showed an out of tolerance condition during the 0.3-s interval. This condition was corrected by connecting a second power supply in parallel through diodes with the existing supply. This increased the OSE supply capability from 12 to 24 A. Procedural changes were also made so that a smooth power switchover from internal to external power could be accomplished.

d. Equipment description.

LTS and STS. The design modifications discussed in *Paragraph c* have only slightly changed the OSE external appearance and functional operation. The LTS consists of two STS racks, including the control and power consoles, and the laboratory adapter rack. The control console assemblies (from top to bottom) are the (1) self-test, (2) counter, (3) transfer, (4) control panel, (5) clock, (6) scanner control, (7) crossbar scanner, (8) multimeter, and (9) recorder. The counter is a new assembly that has been added to this console.

The power console assemblies (from top to bottom) are the (1) auxiliary power supplies, (2) switching-logic, (3) test monitor, and (4) dual power-source simulator. A spacecraft ground connection has been brought to the panel to allow measurement of battery leakage. A new multiposition rotary switch with additional positions is now used to select 16 different commands. Three push-button switches were added to the panel for the

Mariner Mars 1969 heater loads. The portion of the panel with seven rotary switches for dummy loads has been modified to five switches and a spare.

The LAR assemblies (from top to bottom) are the (1) RFS–battery (new), (2) true rms voltmeter, (3) oscilloscope, (4) Case I test (new), (5) Case VIII test (new), (6) 2.4 kHz power supply, and (7) 4A19 fuse monitor (new). The new *RFS–battery assembly* contains the dummy load resistors to simulate the radio subsystem load on the primary dc bus. These resistors simulate the spacecraft radio subsystem dc load currents in the spacecraft power source and logic module.

The new *Case I test assembly* provides the power source, control, monitoring, and loading for the Case I power conditioning assembly. All functions are provided so that Case I may be given functional, FA, TA, and life tests. A switch on the panel controls the power distribution relays. Test points are provided to connect the oscilloscope and rms voltmeter for measurements.

The new *Case VIII test assembly* provides the power source, control, monitoring, and loading for the Case VIII booster regulators. Again, all functions are provided so that Case VIII may be given functional, FA, TA, and life tests. Controls used in the system test mode of operation and available in other parts of the OSE are routed to this assembly for testing Case VIII. Test points are available in the assembly to calibrate the telemetry channels, verify the battery charger operation, and observe the booster operation in the share mode. The 2.4-kHz power supply powers Case VIII when Case I is not used.

The new *4A19 fuse monitor assembly* provides test points to measure the voltage on the load side of the fuses in the flight power distribution module. Test points are also provided for the radio subsystem dc power telemetry transducer.

LCE. The launch control panel assembly is similar in appearance to the power control assembly in the STS. Two switches, the main-transfer and the standby-transfer, were added to the front of the panel, and a toggle switch was added behind the panel to switch the range of the ammeter. The power control assembly and a digital multimeter are mounted in the two LCE racks along with the other CC&S, attitude control, and scan LCE.

The power console is located in the launch complex transfer room and the ac–dc conditioner assembly is mounted in a junction box located in the umbilical tower. The LCE assemblies (from top to bottom) are the (1) auxiliary power supplies, (2) transfer, (3) self test, (4) power control, (5) dual power-source/simulator, and (6) power distribution.

A buffer was added in the ac–dc conditioner assembly to monitor the spacecraft 2.4 kHz power supply.

Calibration test set. The calibration test set consists of the FPS simulator and the solar panel simulator calibrator. The solar panel simulator calibrator has been used on previous programs to calibrate the simulators in the OSE for the desired solar panel characteristic. There have been few modifications to the calibrator since it was designed.

The FPS simulator was modified for *Mariner* Mars 1969 from selected lab equipment. The FPS simulator assemblies (from top to bottom) are the (1) precision rms voltmeter, (2) differential voltmeter, (3) oscilloscope, (4) dc simulation control, (5) ac simulation control, (6) 2.4-kHz power supply, and (7) dc power supply.

The FPS simulator is used as a parameter and interface standard for checkout of the OSE and to calibrate sensors and detectors. The assembly names indicate the simulator functions, types of compatibility measurements, and calibrations possible with this equipment when used in OSE checkout. After the OSE has passed the simulator procedural operations, a 100-h burn-in, and a compatibility test with a flight equipment prototype or equivalent, it is ready for use with flight power equipment. The FPS simulator is also used to train OSE operators in the operation of the OSE.

3. Far Encounter Planet Sensor

a. Introduction. The far encounter planet sensor (FEPS), an electro–optical device, will be employed during the far-encounter phase of the *Mariner* Mars 1969 spacecraft mission. The FEPS provides two-axis pointing signals to the scan control subsystem to direct the spacecraft scan platform at the center of the illuminated portion of the planet Mars during the far-encounter phase of the mission. The two pointing (error) signals are proportional to the displacement between the center of the illuminated portion of Mars and the FEPS optical axis. The FEPS also produces an electrical signal that will indicate when Mars is within the FEPS field-of-view. The high-resolution TV camera and the FEPS, mounted on the scan platform, are boresighted together.

b. Operational description. Light from Mars enters the objective lens of the FEPS and is focused on detectors in two different locations by means of a beam-splitting mirror. Each of the two silicon photovoltaic detectors is a dual unit consisting of two half cells. The half cells are sequentially connected to a single amplifier by a multiplex (time-shared) modulator so that a simple radiometric balance is obtained in each control axis when the FEPS is properly pointed at the radiometric centroid of Mars. The tracking transfer function is 10 V/deg over tracking error angles of ±1 deg. A saturated output is maintained out to ±5 deg.

Automatic gain control (AGC) is provided by means of pulse-width modulation of the samples from the detector half cells. The AGC is required because the planet diameter changes from 0.285 to 1.40 deg during the far-encounter phase as the spacecraft approaches Mars. The change in the FEPS illuminance may be as much as 24.2:1. The AGC signal is derived from the sum of the four half-cells outputs.

A planet-in-field-of-view (PIFOV) signal is derived from the AGC signal to act as a thresholded indication that the FEPS is functioning and that the error signals are available for controlling the scan platform servo system. The error signals are conventional phase-reversing dc signals, and the PIFOV signal is a level change from 0 to approximately 4.6 V. There are no moving parts in the FEPS. Both 2400 Hz square-wave power and 15-Vdc power are used.

Table 10 provides a listing of the nominal FEPS parameters. A simplified schematic of the FEPS, consisting of lens, beam splitter, detectors and processing electronics, is shown in Fig. 13.

c. Electro–optical description. The FEPS configuration is shown in Fig. 14. The unit has an approximate 12-in. overall length and 3-in. diam. The exploded view in Fig. 15 shows all the major subassemblies that make up the FEPS. The heart of the sensor is the beam-splitter and detector assembly. This assembly houses both silicon detectors and the polka-dot beam splitter. The beam splitter slides into the main housing and is positioned with respect to the lens (focus) by means of a threaded rod connected to the main housing. Built into the beam-splitter housing are the translational and rotational adjustment devices for the silicon detectors. By providing translational and rotational adjustment of the detectors with respect to the boresight axis of the sensor, the detector bisecting line can be made to fall exactly on the optical axis and thereby greatly reduce null errors and increase overall pointing accuracy.

Table 10. Nominal FEPS parameters

Parameter	Description	Parameter	Description
Error signals		**PIFOV signal**	
Signal type	Dc analog	Signal type	Dc digital
Error output	Two axis	Signal magnitudes	4.6 ±0.5 V (PIFOV)
Total range (saturated)	±5 deg		−0.5 ±0.5 V (no PIFOV)
Linear range	±1 deg	Output impedance	5 kΩ
Linearity	0.3 V/deg	Time delay (turn off)	1 s
Scale factor	10 V/deg ±30%		
AGC range	25:1	**Miscellaneous**	
Frequency response (−3 dB)	10 Hz		
Phase shift	6 deg at 1 Hz	Power consumption	0.75 W
Output impedance	1 kΩ	Weight	2.3 lb
Threshold and resolution	0.01 deg	Volume	75 in.^{3}
Accuracy	0.2 deg		
Channel separation[a]	43 dB		
Mounting alignment (around LOS)	0.4 deg		

[a]Corresponds to an orthogonality of 0.4 deg.

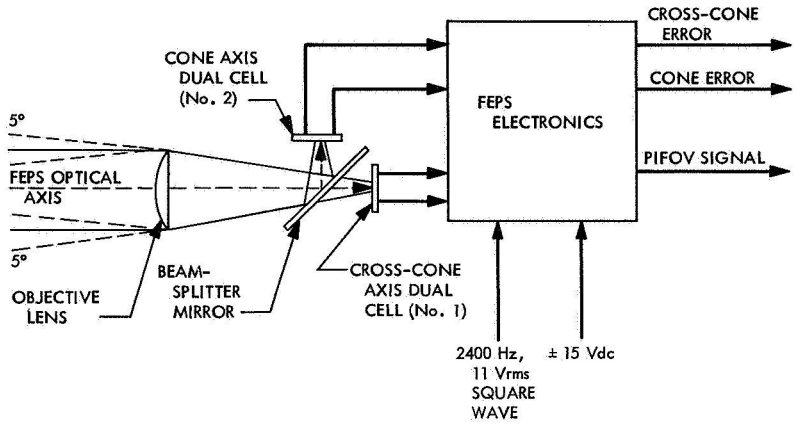

Fig. 13. FEPS simplified schematic

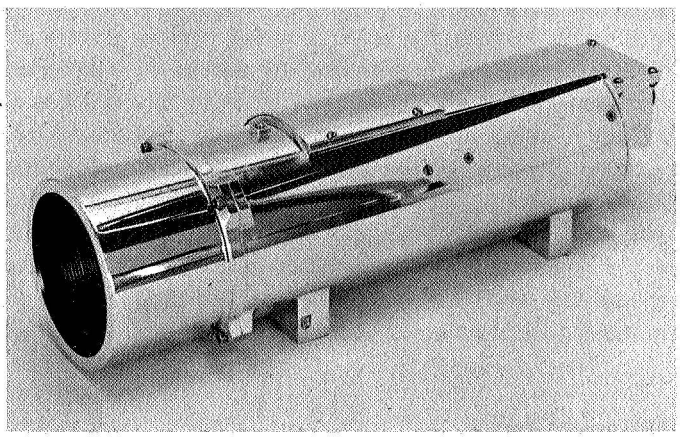

Fig. 14. FEPS mechanical configuration

Objective lens. The objective lens is plano–convex with a 3.5-in. effective focal length (EFL) and a 2.0-in. effective diameter. The lens is fabricated from fused quartz and coated with an anti-reflection coating of magnesium fluoride.

Beam splitter. A high-efficiency beam splitter, angled at 45 deg to the optical axis, lies immediately behind the objective lens. This beam splitter consists of a 0.062-in. fused quartz plate with a polka-dot mirror surface. These polka dots are vacuum-deposited aluminum and act as individual mirrors. Each dot has a 0.049-in. diam and is deposited in a rectangular grid pattern. The ratio of reflecting area to transmitting area is adjusted to evenly divide the radiant energy between the two detectors. Both surfaces of the beam splitter are coated with an anti-reflective coating of magnesium fluoride to minimize reflective losses.

Detectors. The FEPS detectors (there are two detectors per FEPS) are circular photovoltaic silicon cells with an approximate 0.6-in. diam. The detector diameter and lens EFL combine to define the FEPS field-of-view, which is a 10-deg circular cone. The dual feature of the detector is obtained by producing a mesa-etched border and dividing line, which delineate the active cell areas and provide a common anode. The cathode leads are soldered to an electroless nickel solderable area deposited around the detector periphery.

The silicon detector is fabricated from N on P, 10-Ω-cm material since this material has the highest radiation resistance and gives good performance at low lights levels. The diffusion depth was chosen for maximum voltage output rather than maximum power output as required for solar cells.

d. Electronics general operation. The complete FEPS electronic block diagram is presented in Fig. 16. A very general description of FEPS circuit operation follows.

The FEPS electronics sample a complete set of detector output voltages 600 times a second. The amplitude of each sample is analogous to the irradiation of the corresponding sector. The AGC is accomplished by reducing the width of the sampled pulses. The 2400-pulses/s pulse train is then ac amplified and distributed to three demodulator circuits. One demodulator operates synchronously at the 2400-Hz rate to generate an AGC voltage. A low-pass filter removes the ripple component, giving a voltage that is an analog of the total irradiance within the field-of-view. This voltage then goes to a pulse-width modulator that establishes the width of the sampling pulses.

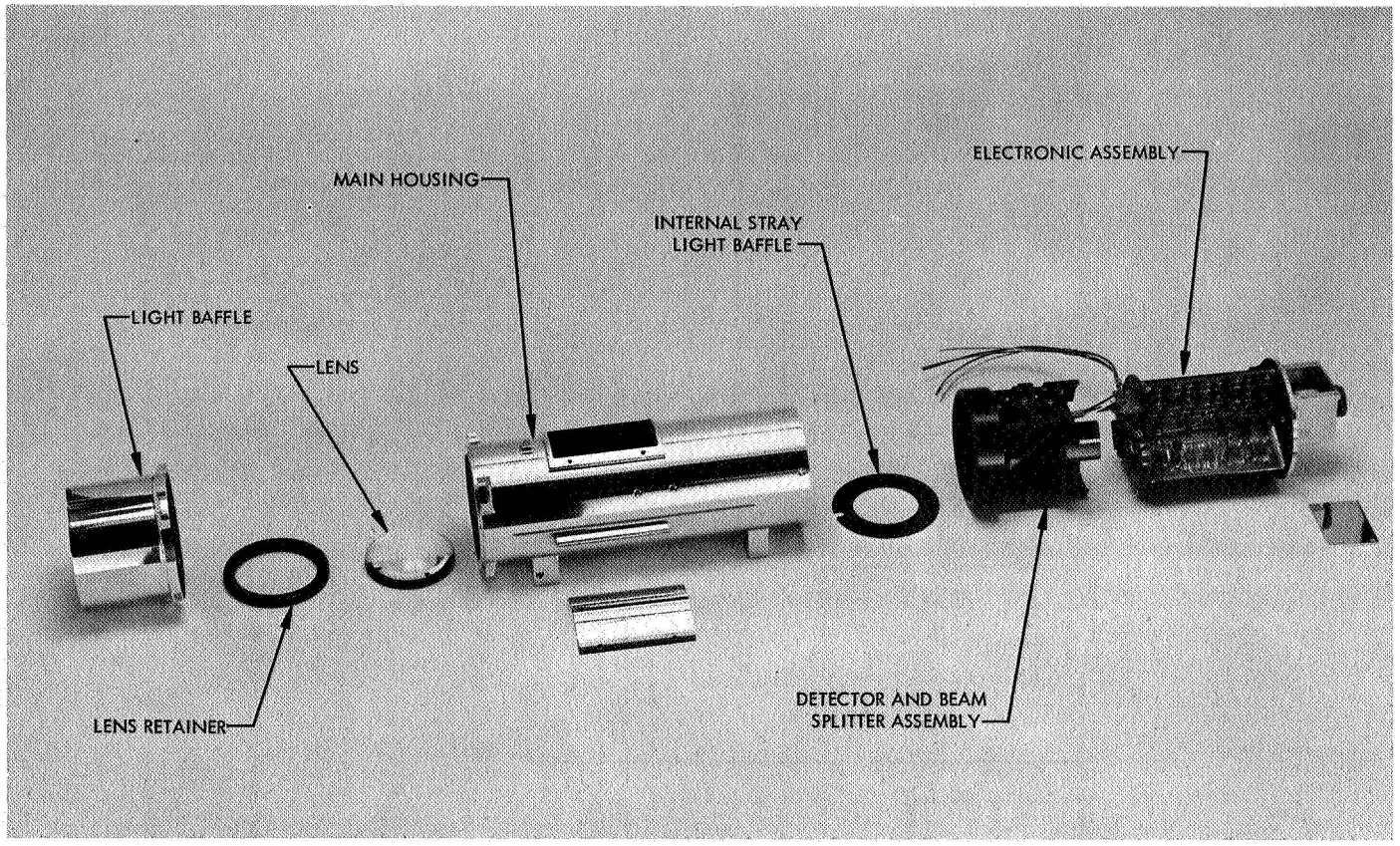

Fig. 15. FEPS subassemblies

The amplified signal is also fed to two identical demodulator/output amplifier circuits. The demodulator in each is driven by the same logic that samples the detector voltages. The demodulation generates a voltage proportional to the difference in the areas of corresponding pairs of pulses. This voltage is then dc amplified and filtered by the output amplifier. This amplifier is connected to operate as a filter with a break frequency of approximately 14 Hz. The smoothed output voltage is an analog of the angular error and has a tracking transfer function of approximately 10 V/deg.

e. Sensor performance. All of the original design parameters were met or exceeded by the FEPS flight units. Following the completion of the last unit, the far-encounter flight sequence was changed. The original dynamic range of operation was from encounter (E) minus 48 h ($E-48$ h) to $E-12$ h. (The FEPS was designed for this range.) The new range is to be $E-76$ to -4.5 h. Therefore, a series of tests was performed to determine the FEPS operating characteristics with respect to the new range of operation. It is concluded that satisfactory operation of FEPS can be obtained from $E-76$ to -7 h for all three flight units. Two of the flight units can also perform satisfactorily down to $E-4.5$ h, which meets the desired performance. Although the sensor was not designed to meet the accuracy requirements at $E-4.5$ h, it will function with sufficient accuracy to orient the TV camera toward the planet and allow satisfactory picture coverage.

F. Telecommunications

1. Ground Command Subsystem

a. Introduction. The *Mariner* Mars 1969 ground command subsystem (read, write, and verify [RWV]) is the terminal equipment used to generate 26-bit commands necessary for radio control of the spacecraft.

The RWVs are used at JPL and the Air Force Eastern Test Range (AFETR) for all system test operations and will be used at each committed deep space station (DSS) to generate command modulation signals for commanding the spacecraft(s) during the mission.

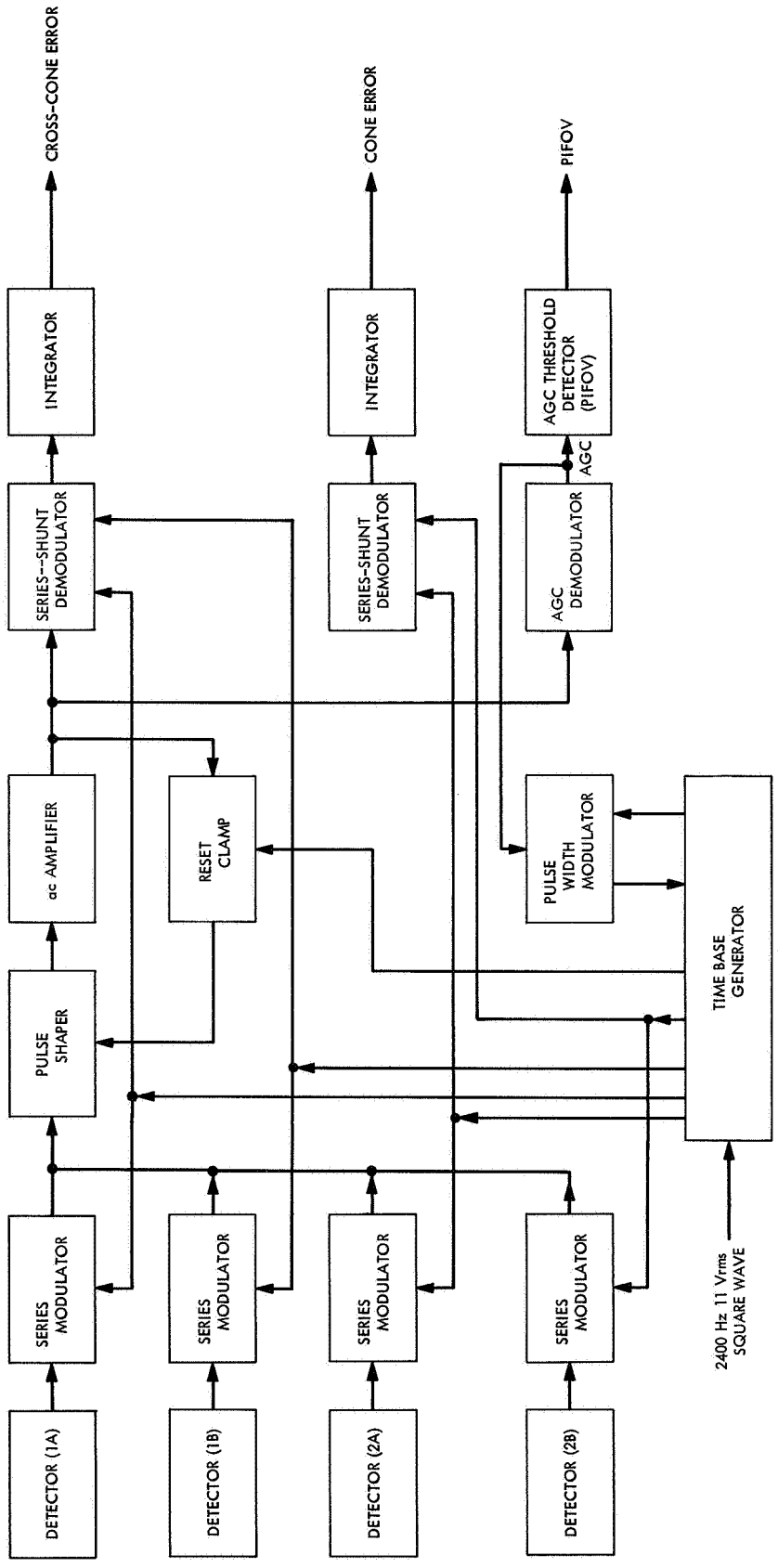

Fig. 16. FEPS electronics block diagram

The RWVs were originally designed and built by Astrodata Corp. in the early 1960s. Since its inception, the RWV has been used to support *Rangers III* through *IX*, as well as all of the *Mariner* projects. A description of the RWV as it was during the *Mariner* Mars 1964 Project is given in Ref. 1. The *Mariner* Venus 67 version of the RWV is discussed in Ref. 2.

In 1967, the decision was made to modify the RWVs for use on the *Mariner* Mars 1969 Project. A contract was awarded to Motorola, Inc., for the design and fabrication of modification kits that would provide the RWVs with a mode of operation compatible with the *Mariner* Mars 1969 requirements while maintaining the capability to support the *Mariner* Venus 67 Project. These requirements were met and the kits have been installed and tested.

A basic block diagram of the RWV is shown in Fig. 17.

b. Functional requirements. The functional requirements of the RWV are as follows:

(1) To read and display incoming command information and verify through redundancy that it is correct.

(2) To convert the incoming information to a form suitable for transmission to the spacecraft.

(3) To verify through the use of the converted information that the RWV internal circuitry is functioning correctly.

(4) To supply modulation to the transmitter, using the converted information, and verify that the modulated signal is correct. If the modulated signal is incorrect, modulation will be coded in a manner that will cause the spacecraft to ignore the command.

(5) To write the transmitted signal by means of a punched paper tape.

(6) To write tape information suitable for transmission to the spacecraft on punched paper.

(7) To allow command transmission to be initiated, either manually or automatically, by an external time source.

(8) To provide an emergency mode of operation such that either a power supply failure or a failure in a non-critical circuit will not prevent command transmission.

c. Overall operation. A command to the spacecraft is read into the RWV via its paper-tape reader. The command is processed by the RWV and is combined with a synchronization signal to form a composite command signal that modulates the ground transmitter. Internal command processing consists of checking the tape input for parity errors; circulating the command through the same registers and signal paths that are used during transmission (in order to check the RWV for proper operation); generating the command modulation, synchronization signal, and the composite command signal; monitoring the modulator output in real time (to detect errors during transmission); and punching the transmitted command onto an output paper tape. The RWV consists of seven chassis bays of electronic logic, various control panels and displays, a variable oscillator, a paper-tape reader and punch, power supplies, an oscilloscope, and an electronic counter.

d. Operational capabilities. The RWVs are capable of various modes of operation. Basically these modes are: (1) mode 1, which checks the punched paper tape received over the teletype lines, (2) mode 2 verify, which checks the internal operation of the RWV but without actually transmitting a command, and (3) mode 2 transmit, which actually transmits a command. The RWVs are also capable of initiating and transmitting a command in an automatic and an emergency mode. A more detailed description of these modes of operation is presented in the following paragraphs.

Mode 1 verify. Mode 1 is used to verify the command as received on the teletype. This command is always in the form of three identical words on punched paper tape. Mode 1 will read all three words, check each for parity, check each word against the other two for identity, perform certain checks of the internal logic of the subsystem, and punch the command onto paper tape with the tape perforator.

Mode 2 verify. The primary purpose of mode 2 verify is to verify that the ground modulator and detector are functioning properly. The paper tape input may be either the three-word group used as an input for mode 1, or a single-word command punched at the end of the mode 1 program cycle.

After the paper tape is read, the command is loaded into the A and C registers. The contents of the C register are then shifted into the modulator. The modulator output is connected to the detector input, and the detector output is used as the input to the C register. As the word

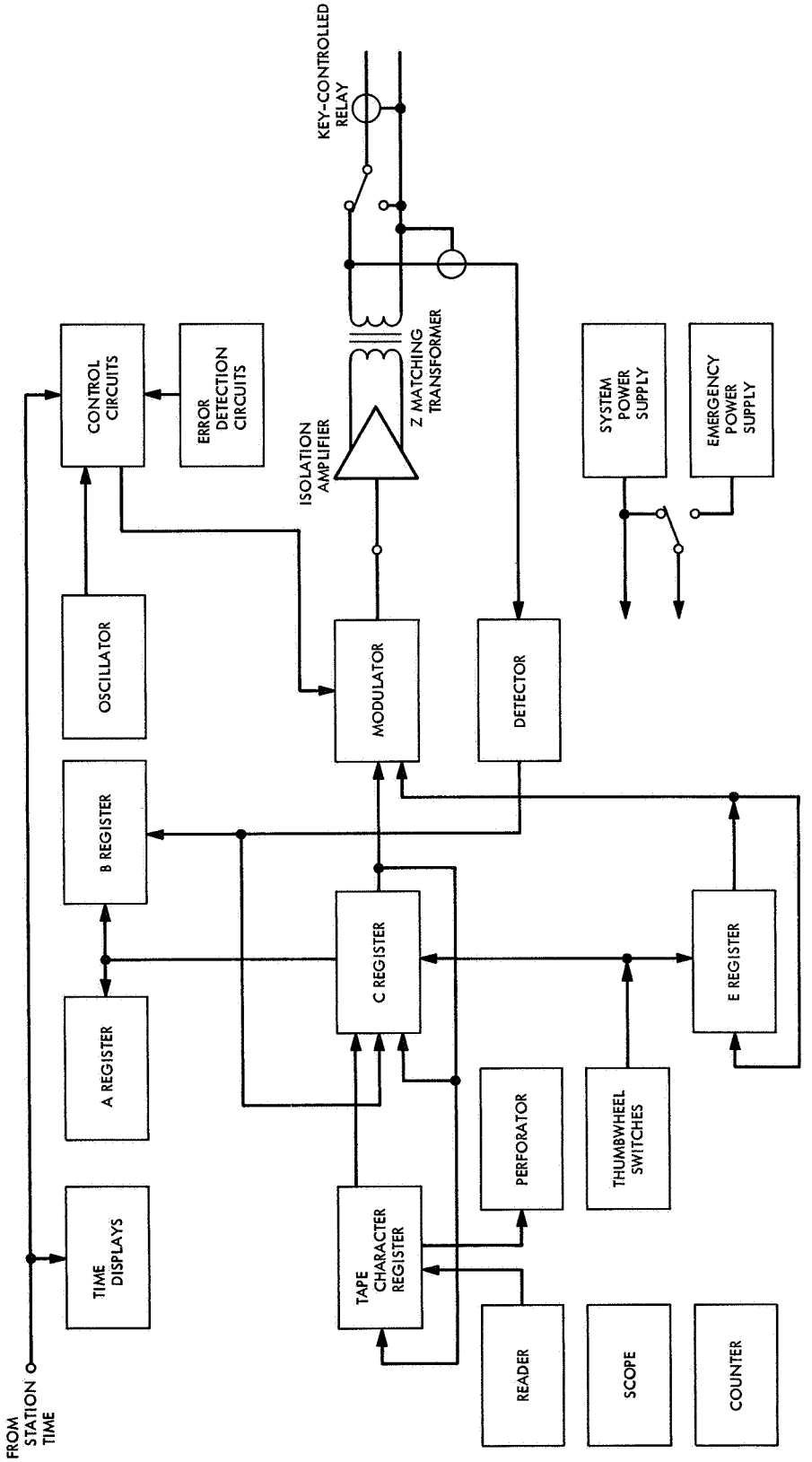

Fig. 17. RWV block diagram

is being shifted into the modulator, the modulator input is compared to the detector output. The contents of the C register (the word returned by the detector) are loaded into the B register, and then the contents of the B register are compared to the contents of the C register. This verifies that the B register was loaded properly. Also, the contents of the A register are compared to the contents of the C register. This verifies that the word returned by the detector is the same as the word read from tape.

Mode 2 transmit. The purpose of mode 2 transmit is to transmit a command. The first portion of mode 2 transmit is identical to mode 2 verify. Where mode 2 verify stops after loading the verified word into the B register, mode 2 transmit continues to the next program step, which again shifts the contents of the C register into modulator. During this step, the modulator output is connected to the transmitter input. During the transmission, the modulator input is again compared to the detector output and the detector output is shifted into the C register. If an error is detected during transmission, the synchronization signal (pseudo-noise code) is inverted for 2 s, which causes the flight command subsystem decoder to be inhibited.

The next step punches the transmitted word onto paper tape and then compares the contents of the A register to the contents of the C register. This verifies that the transmitted word was identical to the word read from the tape.

Automatic (timed start). A timed-start feature is incorporated into the RWV that permits the start of an operation at a specified time of day. The desired start time (in hours, minutes, and seconds) is set on the thumbwheels on the system control panel and the INITIATE switches are activated. When the clock time coincides with the time set on the thumbwheel, the RWV will automatically start its operation. The timed-start feature can be used with modes 1 and 2.

Emergency operation. The emergency mode of operation provides a means of transmitting a command in the event of a system malfunction or system power-supply failure. In the emergency mode, power is applied only to the circuits containing the minimum logic necessary to transmit a command. Under this condition no command verification or error detection takes place, i.e., no inversion of the sync signal. In the emergency mode, the desired command is set on the MANUAL INPUT thumbwheel switches. When the INITIATE button is depressed and released, the command is transmitted immediately.

e. **Mariner *Mars 1969 logic modification.*** Those areas in which the detailed logic of the *Mariner* Mars 1964–*Mariner* Venus 67 configuration is changed are included in the following description of the *Mariner* Mars 1969 modulation-configured RWV.

The command subcarrier for the *Mariner* Mars 1964 and *Mariner* Venus 67 spacecraft was a modulation signal of cos $2\pi(2f_s)t$, whereas the command subcarrier for the *Mariner* Mars 1969 modulation signal is a sin $2\pi(f_s)t$ signal.

The phase of a $2f_s$ square-wave signal remains constant with respect to the bit-sync pulse, while the phase of a f_s square-wave signal changes 180 deg for each consecutive bit-sync pulse. Because of this phase ambiguity in the *Mariner* Mars 1969 command subcarrier, the flight command subsystem logic is designed to force the phase of the command demodulator reference (f_s square-wave signal) to be set unambiguously at each bit-sync time. This method cannot be used in the RWV, since the sinusoidal subcarrier must be developed from the reference f_s square-wave signal. Instead, the phase relationship between the modulating data and the f_s subcarrier is established unambiguously by determining and storing a binary indication of the phase of the f_s subcarrier at bit-sync time and then using the stored state to steer either the data bit or its complement to the modulator input. The result is that with bit sync defined as $t = 0$, a "1" data bit is always a sin $(2\pi f_s t + 0°)$, and a "0" data bit is always a sin $(2\pi f_s t + 180°)$signal.

The uncommanded state (rest) is defined as data equal to binary zero. In the *Mariner* Mars 1964–*Mariner* Venus 67 configuration, the output of a $2f_s$ sine-wave shaper drives a phase-shift keyer, and, in addition, is linearly summed with the synchronization signal to generate the uncommanded composite modulation. This can be done because the in-phase $2f_s$ sine-wave signal represents binary zero. In the *Mariner* Mars 1969 configuration, the binary zero data is in phase with the f_s sine-wave signal only one-half of the time. As a result, a second phase-shift keying circuit is provided to generate the data portion of the uncommanded composite modulation. The active phase-shift keying circuit cannot be used to generate the rest data due to the internal self-checks performed just prior to transmission in the RWV.

The portion of the composite signal used by the spacecraft for establishing sync is defined as the time-varying function PN $\oplus$ $2f_s$, where PN is the pseudo-noise code

and the symbol $\oplus$ denotes a half-adder. Operation of the *Mariner* Mars 1969 flight command subsystem (FCS) decoder inhibit function is such that the inverted function, $\overline{PN} \oplus 2f_s$, must be generated by the RWV and substituted for the normal synchronization signal when an RWV-originated error is detected. This inverted function causes the FCS decoder to be inhibited.

The FCS decoder inhibit function is initiated by inverting the synchronization signal for two bit times. The same logic conditions cause the *Mariner* Mars 1969 and the *Mariner* Mars 1964–*Mariner* Venus 67 error-detection circuits to assume the set state. Once set, the *Mariner* Mars 1964–*Mariner* Venus 67 error-detection circuits remained set (and the RWV modulation output was disabled) until reset by actuation of the ERROR indicator/switch. Reset of the *Mariner* Mars 1969 error-detection circuits is controlled automatically by a sync inversion counter, which also inhibits the occurrence of more than one synchronization signal inversion for the same error occurrence.

The sync inversion counter is a two-stage shift register that detects that sync inversion has occurred and provides a reset function after the sync has been inverted for two bit times. The *Mariner* Mars 1969 RWV detector data demodulator is the same as the *Mariner* Mars 1964–*Mariner* Venus 67 detector data demodulator, except the center frequency has been changed from $2f_s$ to f_s and that various circuits are clocked at an f_s rate.

The RWV detector also checks the composite modulation for the proper synchronization signal. The composite signal is bi-phase modulated by the detector time-varying signal $PN' \oplus f_s$. The prime sign is used to denote the detector pseudo noise. The output of this demodulation process, when the detector is locked to the composite signal, is a square-wave signal at frequency f_s and lags the RWV modulator reference f_s by 90 deg. The output is filtered to obtain a sine-wave signal at frequency f_s; the phase of this sine-wave signal is then advanced 90 deg. The zero crossovers of the resultant signal ($f_s < 0°$) provide the reference to which the detector voltage-controlled oscillator (VCO) is phase-locked. The VCO output frequency is divided to obtain square-wave signals $2f_s$ and f_s. The intermodulation components resulting from the *Mariner* Mars 1969 command subcarrier, bi-phase modulated by $PN' \oplus f_s$, generate a significant phase error in the detector VCO loop. To alleviate this problem, the *Mariner* Mars 1969 configuration includes a bandstop filter tuned to f_s to remove the command subcarrier from the composite modulation signal prior to demodulation of the synchronization signal.

f. Conclusion. The RWV logic has been modified and is now compatible with the *Mariner* Mars 1969 spacecraft requirements. In addition to the logic modification, the following five additional changes have been incorporated in the RWVs since *Mariner* Venus 67 operations:

(1) Relocation of the tape perforator. This change was added primarily for operator convenience.

(2) Deletion of the S-band monitor receiver. Sampling of the transmitted S-band signal for error detection purposes is not required for *Mariner* Mars 1969.

(3) $32f_s$ logic modification. This was a minor correction to the logic to eliminate a $32f_s$ signal from the composite output.

(4) Deletion of command word format decal. This change deleted a front panel breakdown of the *Mariner* Venus 67 command word.

(5) Binary command output. This modification provided the binary command output to the station oscillograph for recording purposes.

The present plan is that the multiple-mission command system will replace the RWVs on all projects subsequent to *Mariner* Mars 1969. The RWVs have been supporting JPL projects since 1962 and retirement of the hardware is considered warranted.

References

1. *Mariner Mars 1964 Project Report: Mission and Spacecraft Development: Volume I. From Project Inception Through Midcourse Maneuver,* Technical Report 32-740, pp. 415–417. Jet Propulsion Laboratory, Pasadena, Calif., Mar. 1, 1965.
2. *Mariner Venus 67 Final Project Report: Volume I. Launch Through Midcourse Maneuver,* Technical Report 32-1203, pp. 393–396. Jet Propulsion Laboratory, Pasadena, Calif., June 15, 1968.

2. Flight Command Subsystem Operational Support Equipment

a. Introduction. The operational support equipment (OSE) for the *Mariner* Mars 1969 flight command subsystem (FCS) consists of four double-rack consoles, four bench-test fixtures (BTFs), and one auxiliary console. The OSE either tests the FCS as an integrated unit or

tests the individual subsystem functional elements (command detector, command decoder, and transformer–rectifier). The OSE generates all programmable commands and signals, including power, used by the FCS and receives, decodes, and monitors the outputs from the FCS. It also displays signal outputs and provides a printout of error data.

A block diagram for the FCS OSE is shown in Fig. 18. A block diagram for the auxiliary console is shown in Fig. 19.

b. FCS OSE test capabilities. The following paragraphs contain a discussion of the five OSE test capabilities and the methods of connecting the FCS to its OSE.

Bench test. The FCS is plugged into the BTF chassis. The OSE generates all signals and programmable commands required by the FCS. The BTF chassis allows the FCS to be installed in any type of environmental chamber.

Three types of bench tests can be performed on the FCS: (1) tests of the decoder at normal bit rate with the detector connected, (2) tests of the decoder at four times the normal bit rate with the detector bypassed, and (3) tests of the detector. Special tests that can be performed in the bench-test configuration are (1) detector correlation, (2) detector bandwidth, (3) word start error, and (4) bit error.

Functional element test. Any of the three functional elements of the FCS (command detector, command decoder, and the transformer–rectifier unit) are plugged into the functional element test (FET) drawer. The auxiliary console is used in this configuration.

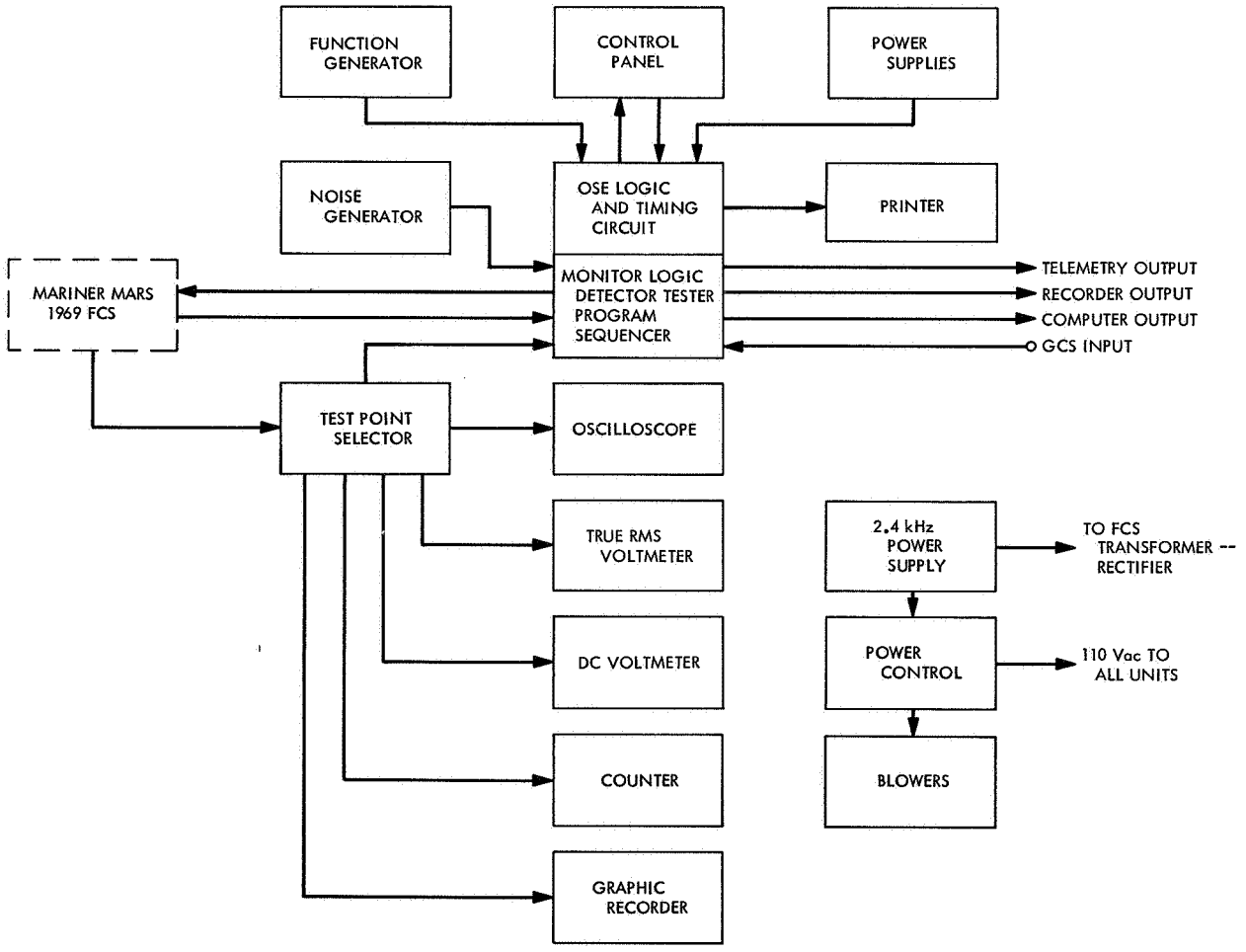

Fig. 18. OSE block diagram

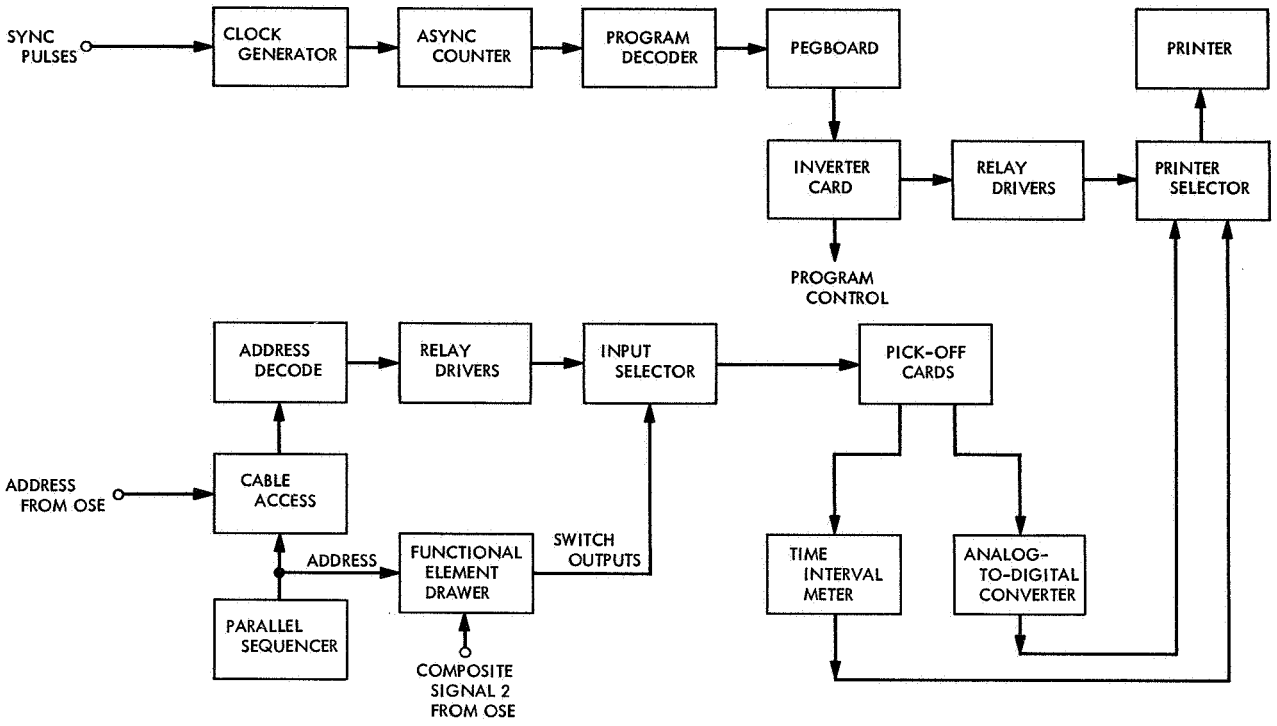

Fig. 19. Auxiliary console block diagram

Tests of the command detector and command decoder are performed in the bench-test configuration as described above. The transformer–rectifier is tested separately. Maximum and minimum loads are applied and the output voltages measured.

Data logging test. The FCS is plugged into the BTF chassis or the FET drawer, which is connected to the data logging input of the auxiliary console. The prime purpose of the auxiliary console is to automatically measure five parameters of the FCS switches. The results are printed to provide a permanent record of the measurements. This process is called data logging. The data logging test is controlled by a program sequence generated by the OSE or by a sequencer in the data logger. The tests performed are (1) leakage current, (2) crest time, (3) rise time, (4) fall time, and (5) saturation voltage.

The leakage-current and crest-time measurements are made with a minimum load, and the rise-time, fall-time, and saturation-voltage measurements are made using a maximum load.

SAF monitor. All connections to the FCS are made via the Spacecraft Assembly Facility (SAF) cables. The primary purpose of the OSE in SAF (or in any systems testing) is to monitor the FCS direct-access test points with the ground command subsystem (GCS) generating the commands. The OSE receives the command bits generated by the GCS and compares these bits with the response from the FCS. The TRANSMITTED ADDRESS and SUBADDRESS displays show the command address sent by the GCS. The RECEIVED ADDRESS and SUBADDRESS displays show the command addresses received by the FCS. A visual comparison of the addresses may be made; however, each command sent by the GCS and the results of the test-point monitoring of the FCS are recorded on the OSE printer.

SAF test. All connections to the FCS are made via the SAF cables. The purpose of the OSE in the SAF test mode is to send commands to the FCS mounted on the spacecraft and monitor the direct-access test points for proper FCS operation. The FCS is connected to the other subsystems in the spacecraft. The OSE generates the command words and sends the composite signal to the radio frequency subsystem (RFS) OSE for transmission to the spacecraft. The OSE monitors the direct-access test points and records, on the OSE printer, any errors that occur. A special test mode is sometimes used in systems testing with the composite signal hardlined directly to the FCS. This mode allows testing to be conducted without the RFS being used. In this special test

mode, all monitoring of the FCS is the same as when transmitting through the RFS OSE.

c. FCS OSE description.

Detector tester. The detector tester provides five test functions for evaluation of the FCS performance capability and develops the basic timing functions for the OSE. The five detector test functions are (1) signal 1, (2) signal 2, (3) phase-locked loop bandwidth measurement, (4) correlation test, and (5) pseudo-noise (PN) search–lock delay.

Signal 1 is used to drive the ground transmitter modulator, establishing an RF link with the FCS during spacecraft system tests. The signal consists of a phase-modulated command subcarrier plus a PN code half-added to a square wave (of frequency $2f_s$) sync signal at a level manually variable from 0 to 5 Vrms.

Signal 2 is used to simulate the receiver passband output of the FCS detector for bit error tests. The signal consists of a specified composite signal capable of having noise added to it to check the FCS at various signal-to-noise ratios.

The phase-locked loop bandwidth measurement signal is used to establish the threshold phase-locked loop characteristic of the operational system sync channel. The signal is generated by modulating the OSE voltage-controlled oscillator (VCO) clock-source frequency, and interpreted by simultaneously monitoring the loop phase-detector output of the FCS detector.

The correlation test function is accomplished by manually stepping the OSE PN generator out of sync with the FCS PN generator in such a manner that the FCS PN generator is stepped through the entire sequence in order to re-establish sync, while simultaneously monitoring the FCS detector output for false lock indication.

The PN search–lock delay test function is used to ensure that the FCS will not initiate a search mode until at least two PN generator sequences have elapsed after PN lock has been lost. The test function consists of an interruption of the normal PN $\oplus$ $2f_s$ sync signal for two PN periods.

Program sequencer. The program sequencer provides the counters and control logic used to establish the OSE modes of operation. The initial mode of operation is established by front-panel control switches; the order of the rest of the sequence is controlled by the counter logic. The content of the first message to be generated is established by the control-panel data switches with the succeeding messages controlled by the address sequencer register.

Monitor logic. The functions in the OSE provided by the monitor logic are a program counter used to count bit-sync pulses to establish the bit reference position of the OSE, direct command (DC) monitor logic used to monitor the FCS DC outputs in order to detect errors (selected command error or volunteered command errors), quantitative command (QC) error logic used to monitor the FCS QC outputs, coded command (CC) and bit-check logic used to monitor the FCS CC outputs and the FCS detector bit output, and the test-point check logic used to monitor the FCS direct-access test points. The print control logic controls the OSE printer to provide a hard-copy record of FCS operation during test.

d. **Mariner *Mars 1964 and 1969 FCS OSE.*** The basic FCS OSE built for *Mariner* Mars 1964 was subsequently modified for *Mariner* Venus 67 and further modified for *Mariner* Mars 1969. In general, the test philosophy developed for *Mariner* Mars 1964 FCS and OSE remained the same for *Mariner* Mars 1969 FCS and OSE.

The *Mariner* Mars 1969 FCS OSE was evolved from the *Mariner* Mars 1964 FCS OSE by (1) replacing obsolete or worn-out test equipment, (2) replacing the cordwood logic modules with integrated circuits, (3) rewiring the power distribution circuits, control panels, and test-point selector panels, and (4) making circuit and logic changes as required for additional commands, command format changes, and additional display capability.

e. **Mariner *Mars 1969 FCS OSE performance.*** Although the basic performance of the *Mariner* Mars 1969 FCS OSE has been quite good, two persistently occurring problems have caused some delays in test schedules. Specifically, these are problems with (1) printouts (error indications), and (2) the Motorola MC830P-series dual in-line plastic integrated circuits.

As experiments with shielding and input-filter capacitors showed the noise to be due to radiation, the false printout problem was solved for subsystems testing, and partially solved for systems testing, by shunting each signal input with a 0.01-μF capacitor. Occasional noise printouts during systems testing remains the one *Mariner* Mars 1969 FCS OSE problem that has not been completely solved.

Failures of the Motorola integrated circuits have occurred during both systems and subsystems testing. While the number of failures is not large, they have been difficult to troubleshoot because they are usually intermittent in nature. Under ordinary circumstances, the problem is corrected by isolating the failure to an individual circuit board, and then replacing the entire board while continuing the testing.

II. *Mariner* Mars 1971 Project

PLANETARY–INTERPLANETARY PROGRAM

A. Introduction

1. Mission Description

The primary objective of the *Mariner* Mars 1971 Project is to place two spacecraft in orbit around Mars that will be used to perform scientific experiments directed toward achieving a better understanding of the physical characteristics of that planet. Principal among these experiments are measurements of atmospheric and surface parameters at various times and locations to determine the dynamic characteristics of the planet. Approximately 70% of the Martian surface will be observed during a minimum of 90 days of orbital operations.

During Mission A, it is planned to map the topography of a large portion of the Martian surface at a resolution significantly higher than that achievable with earth-based methods or by the *Mariner* Mars 1969 spacecraft. In addition, measurements will be made of the composition, density, pressure, and thermal properties of the planet's atmosphere. Other measurements will be directed toward an understanding of Mars' surface temperatures, composition, and thermal properties (particularly at the polar caps); its apparent lack of internal activity, its mass distribution; and its shape.

During Mission B, data will be sought on time-variable features of the Martian surface associated with the wave of darkening wherein both seasonal and secular changes occur. Also, information on atmospheric structure and gross dynamics will be obtained, as well as information directed toward an understanding of Mars' mass distribution, its shape, and its apparent lack of internal activity.

A capability will exist to redirect goals for either mission to the alternate mission if desired. The two launches are anticipated for May 1971, with arrival at the planet during the following November.

An engineering objective of the project is to demonstrate the ability of the spacecraft to perform orbital operations in an adaptive mode wherein information from one orbital pass is used to develop the operations plan for subsequent orbital passes. If sufficient resources are available, the necessary modifications will be made to extend the useful lifetimes of the spacecraft past the required 90 days.

One of the *Mariner* Mars 1971 flight spacecraft will be new, and the other will be the spare flight spacecraft of the *Mariner* Mars 1969 Project modified to meet the requirements of the 1971 missions and to enhance mission

reliability. The proof test model spacecraft of the *Mariner* Mars 1969 Project will be modified to become the proof test model for the *Mariner* Mars 1971 Project, to be used for preliminary testing and as a simulator in support of flight operations. A major modification for the *Mariner* Mars 1971 mission will be the addition of a rocket motor required to decelerate the spacecraft and place it in orbit around Mars. The spacecraft configuration is shown in Fig. 1.

Separate scientific instrument subsystems will be required to accomplish each of the first seven planned scientific experiments given in Table 1. The S-band occultation and celestial mechanics experiments will require no additional equipment on the spacecraft. Measurements will be made during both the orbital and the cruise phases of each mission.

Management responsibilities for the overall project, the Spacecraft System, the Mission Operations System, and the Tracking and Data System have been assigned to JPL. Lewis Research Center has been assigned management responsibility for the Launch Vehicle System. The launch vehicle will be an *Atlas/Centaur* developed by General Dynamics/Convair.

The *Mariner* Mars 1971 missions will be supported by the Air Force Eastern Test Range launch facilities at Cape Kennedy, the tracking and data acquisition facilities of the Deep Space Network, and other NASA facilities.

Table 1. *Mariner* Mars 1971 scientific experiments

Experiment	Scientific investigator	Affiliation
Television	G. de Vaucouleurs[a]	University of Texas
	J. Lederberg	Stanford University
	H. Masursky	U.S. Geological Survey
	B. Murray	CIT
	W. Thompson	Bellcomm
Infrared radiometer	G. Neugebauer	CIT
Ultraviolet spectrometer	C. Barth	University of Colorado
Infrared interferometer spectrometer	R. Hanel	Goddard Space Flight Center
Charged-particle telescope	J. Simpson	University of Chicago
Dual-frequency receivers	V. Eshleman	Stanford University
X-ray particle detector	J. Van Allen	University of Iowa
S-band occultation	A. J. Kliore	JPL
Celestial mechanics	J. Lorrell[a]	JPL
	I. Shapiro	

[a]Principal investigator.

2. Project Status

Requests for proposals have been issued for most of the spacecraft subsystems, and a major portion of the procurement action for the major subsystems is expected to be completed by April 1969. Test and operations planning has also been initiated. Mission alternates are the subject of continuing analyses. The initial draft of the mission specification has been reviewed by project personnel, and the preliminary scientific experiment requirements have been furnished for use in mission design activities.

A preliminary functional description of the ground command system has been completed as part of the Mission Operations System activities. Orbit determination problems are being investigated, and a technical and management plan for orbit determination software has been released. The *Mariner* Mars 1971 Project will require a computer of third-generation speed and size. A preliminary list of mission-dependent computer programs has been developed.

The Estimated Capabilities Document for the Tracking and Data System has been released, together with a set of baseline hardware and software requirements for the Deep Space Network tracking, telemetry, and command systems. An implementation schedule has been developed that coordinates the activities required to produce Tracking and Data System documentation.

B. Guidance and Control

1. Parametric Investigation of Pressure Vessel Characteristics

A computer program has been developed for rapid evaluation of the main parameters involved in sizing a pressure vessel for an attitude-control system. The program plots the amount of storable propellant using as parameters the maximum allowable pressure and temperature, the filling pressure[1] and temperature, the vessel main dimensions and mechanical characteristics, and the stored gas characteristics.

The program, written for an IBM 1620 computer, might be utilized for other gases and tank materials by changing the input data, i.e., the virial coefficients and the reference density of the gas and the mechanical

[1]The filling pressure of the propellant at ambient temperature corresponds to the maximum pressure at the maximum temperature. The transformation between the two conditions is assumed to be isovolumetric.

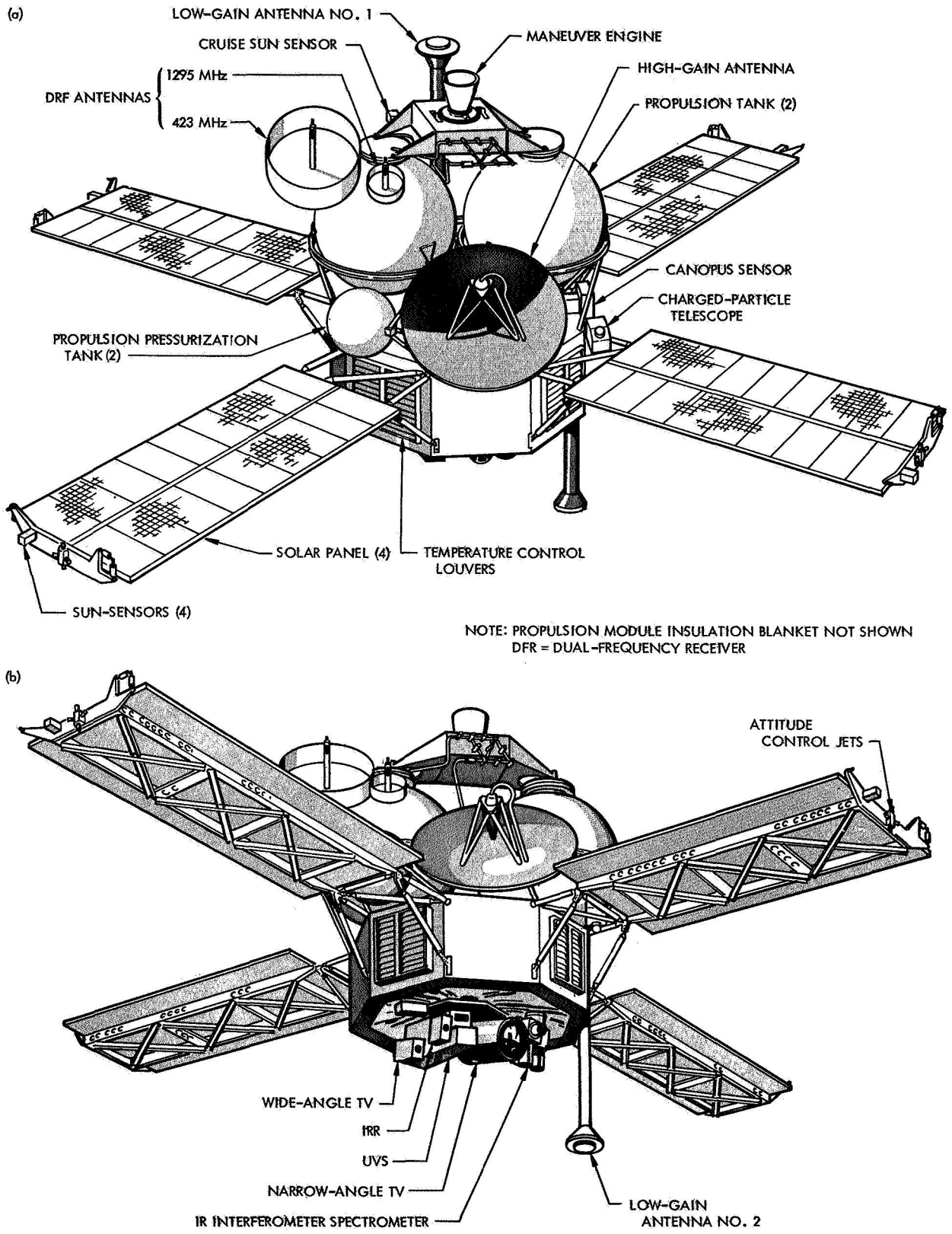

Fig. 1. *Mariner* Mars 1971 spacecraft configuration: (a) top view, (b) bottom view

characteristics of the tank. The temperatures might also be varied to set different boundary conditions.

The type of questions the program will answer are as follows:

(1) Given a pressure and temperature environment, find the amount of gas that can be stored in a vessel of given dimensions.

(2) Given a certain amount of gas, and a pressure and temperature environment, find the main dimensions and weight of the vessel fulfilling the storage requirements.

(3) Find the limits of the possible use of a vessel of given dimensions.

The limits of the investigation are as follows:

(1) The relaxation of the vessel material at the higher temperature has been neglected.

(2) The vessel unit deformation (ε) has been considered only at the first power. Furthermore, the stress concentration over the weldment(s) and neck(s) areas has been neglected, allowing for a slight overestimation of the vessel volume increase under pressure.

(3) The weight of the bottle neck is applicable only to the *Mariner* vessel and is not transferable to other vessel designs without further examination. The same also applies to the weldment reinforcement (considering the vessel obtained by welding together two or more spherical portions).

The results for nitrogen and a Ti6Al4V pressure vessel, between the boundary temperatures T_m = 125°F and T_f = 25°C, are shown in Figure 3 and 4, in which

PM = maximum allowable pressure

PF = filling pressure

MG = N_2 Gas weight

d_i = vessel internal diameter

d_e = vessel external diameter

t = vessel thickness

W_t = tankage weight

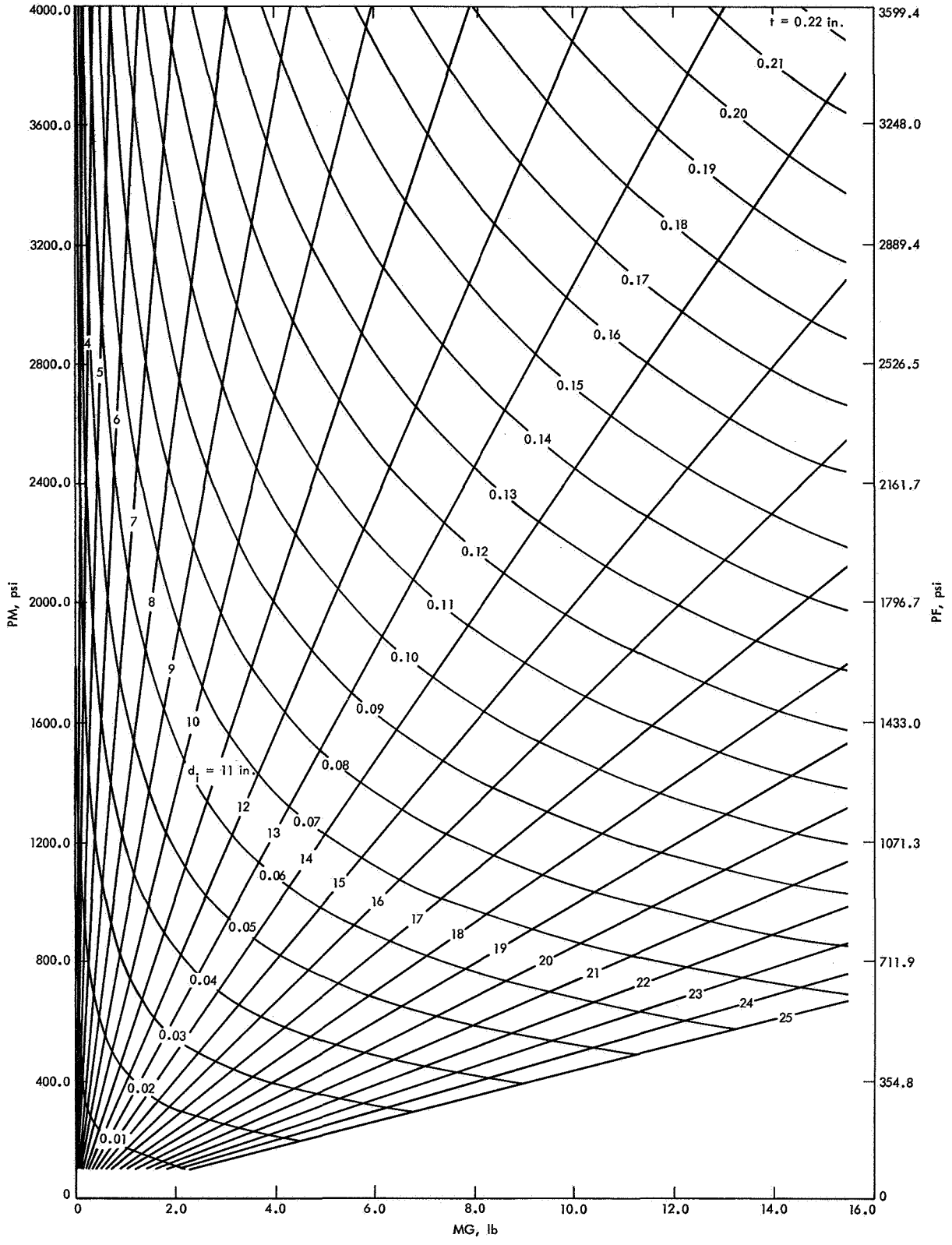

Fig. 2. Pressure vessel d_i and t as functions of *PM* and *PF* versus *MG*

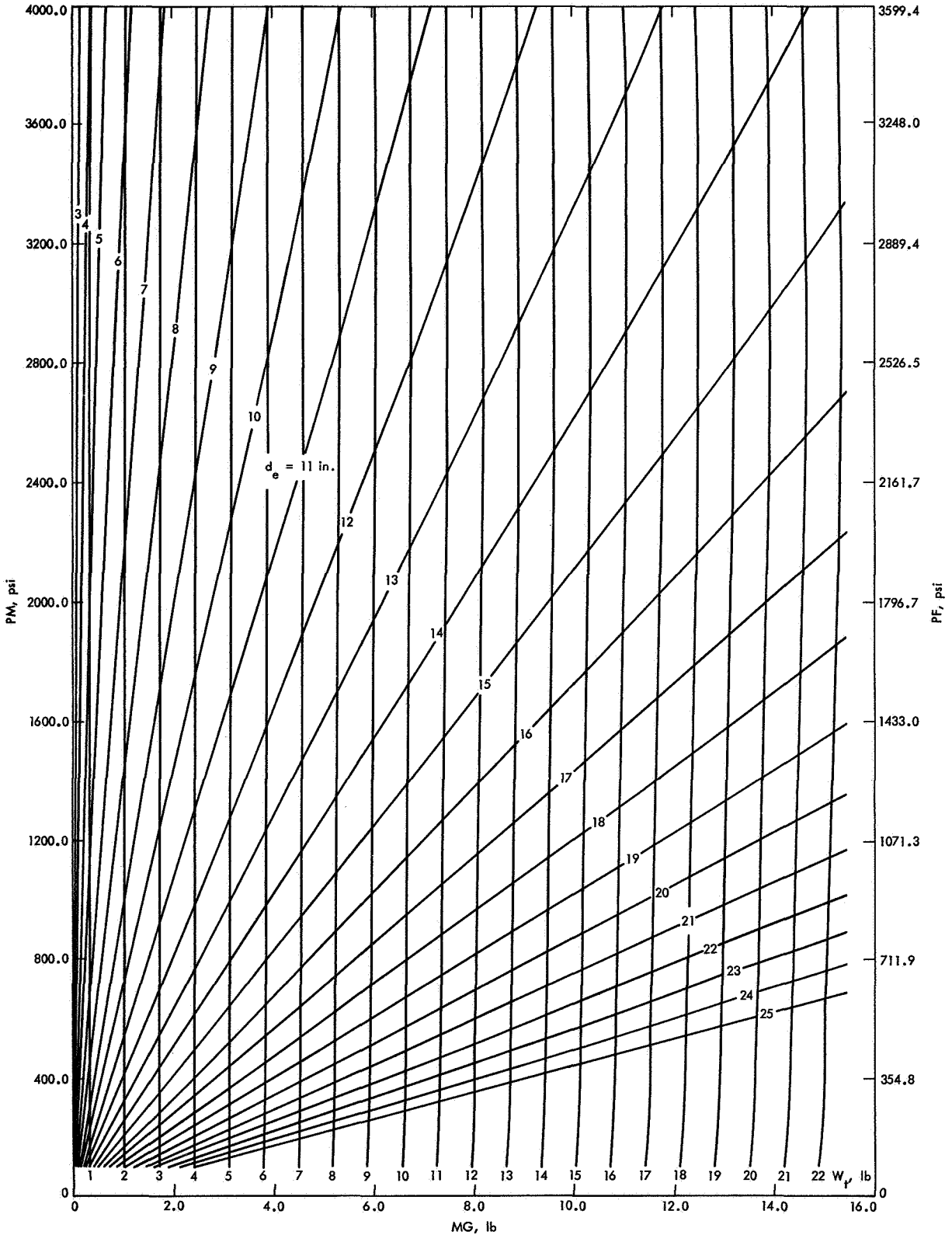

Fig. 3. Pressure vessel d_e and W_t as functions of *PM* and *PF* versus *MG*